NON-LINEAR TRAJECTORY CONTROL OF TENSEGRITY PROSTHETIC (PROTENSE) LEG

A Thesis

by

VISHALA

Submitted to the Office of Graduate and Professional Studies of
Texas A&M University
in partial fulfillment of the requirements for the degree of

MASTER OF SCIENCE

Chair of Committee,	Manoranjan Majji
Committee Members,	Robert Skelton
	Pilwon Hur
Head of Department,	Rodney Bowersox

December 2018

Major Subject: Aerospace Engineering

ABSTRACT

There has been a continuous rise in the number of amputees over the past decades and estimates put the number of amputees in the US alone at over 3 million by 2050. With the rising amputee population, the development of better prosthesis is needed to return quality of life to millions. The field of prosthetic development is active, with improved prosthesis entering the market owing to the advent of new materials and control strategies. The improvement in sensor technology and understanding of the bio-mechanics of the limbs have further bolstered the confidence of engineers to provide prosthetic legs with added power and degrees of freedom allowing the amputees to run faster, trek steeper and scale new heights.

Tensegrity, a word coined by Buckminster Fuller in the 1960s, is an amalgam of the words tension and integrity. A tensegrity structure is a prestressable network of bars and strings with specific boundary conditions and external forces applied at the nodes. Tensegrity structures were introduced as an art form by Kenneth Snelson. Civil engineers paid little attention to the Tensegrity due to absence of a full dynamical model to define it which people like Skelton provided. More recently, the concept of tensegrity became popular with roboticists and control theorists for making complex robots manipulated by strings as actuators. The shape control capability of tensegrity structures without change in stiffness and the capability to provide minimal mass solutions to many engineering problems can be exploited for various applications. In the last 25 years tensegrity has come to be associated with various inquiries into the nature of living structure by Professors like Donald E. Ingber, who has claimed tensegrity to be the best explanation of the working of a cytoskeleton of the cell in his journal, 'The Architecture of life'.

This work describes an initial effort aimed at applying the huge potential of tensegrity structures into the field of leg prosthetics. The objective is to provide a stable and comfortable prosthetic leg for above/below knee amputees with both strong and weak residual leg for motion in the sagittal plane while they walk on level ground.

DEDICATION

To my parents, my brother, my sister, Stefan and Hari.

CONTRIBUTORS AND FUNDING SOURCES

Contributors

This work was supported by a thesis committee consisting of Professor Manoranjan Majji and Robert Skelton of the Department of Aerospace Engineering and Professor Pilwon Hur of the Department of Mechanical Engineering. Financial support was provided by Dr. John Junkins, Dr. Robert Skelton and Dr. Bonnie Dunbar for the completion of my graduate studies.

All other work conducted for the thesis was completed by the student independently.

Funding Sources

Graduate study was supported by a fellowship from Hagler Institure for Advanced Study in collaboration with the TIAS fellow Dr. Robert Skelton.

TABLE OF CONTENTS

Page

LIST OF FIGURES

FIGURE Page

LIST OF TABLES

TABLE Page

1. INTRODUCTION AND LITERATURE REVIEW

1.1 Prosthesis Background

The past decades have seen a rapid growth in capabilities of both replacement prosthetics and augmentative orthoses. In developed countries, the increased demand for prosthetic technologies is primarily due to atherosclerosis and concomitant diabetes, i.e. circulatory dysfunctions that result in amputations. In 2005 there were 1.6 million Americans living with limb loss, of which 54% are owed to vascular disease [1] with trauma related events the second greatest contributing factor (45%), and the number is expected to double to 3.2 million by 2050. From the period 1988-1996, though the rates of amputations in the US due to trauma or cancer have fallen by half, amputations due to vascular diseases like diabetes has grown an estimated 27% [2]. As of 2005, an estimated 185,000 amputations occur annually in the United States [3] with 82% of them due to vascular disease. Studies also indicate that 90% of new amputations concern the lower extremity [4].

In the developing world, the needs arise from industrial and traffic trauma [5], and due to land mines in conflict zones (either military personnel during active duty or displaced civilians returning to land mined zones [6]). The key challenges and constraints of design for defense forces and the physically challenged are much the same - portability and interfacing with a human operator [7]. Recent advances allow amputees with below-calf amputations to return to active life, without a noticeable limp in day to day activities or even compete in professional sport. The remainder of this introduction will focus on developments in prosthetics for lower extremities.

1.1.1 Types of Prosthesis

It is sometimes useful (eg. in forming impact assessments) to categorize prosthesis of lower limbs by degree of amputation, i.e. transtibial (below the knee), tranfemoral (above the knee) and through-the-foot prosthesis. From 1979-1996 the rates of amputations of the lower extremities due to vascular dysfunctions (Diabetic Foot Syndrome) consistently stayed close to the range of 10-12 per 100,000 people for both transtibial and transfemoral cases. The rates of through the foot

amputations are near 7 amputees per 100,000 people [8].

Often, amputees develop further health issues post the amputation as a result of compromised posture and gait. Lower limb amputees have a significantly higher risk of osteoarthritis in the knee and hip of the sound limb. Over 60% also experience back pain within two years of their operation. Hence, prosthetic solutions are constantly evolving towards better bio-mimetic function. The critical components of below knee and above knee prosthesis are the ankle joint and the knee joint, of which we will briefly review available alternatives for which we introduce comparative criteria. Clinical studies comparing prosthetic alternatives map several parameters [9]. These parameters can be grouped into three areas of focus, these are, quality of user's gait with the prosthesis, the degree of effort expended in using the prosthesis, and the aesthetic preferences of users. Below we group some of the major clinically studied parameters in these three themes.

1. **Gait quality** - Stride length, walking speed, cadence [10, 11, 12].

2. **Patient strain/energy consumption** - Heart rate, VO_2 (oxygen uptake), muscle/joint power output [13, 14, 15].

3. **Patient preference and comfort**- Aesthetics, human-likeness, ease of wear [16, 13] .

The parameters mentioned are by no means exhaustive. However, limiting to three key themes provides us with a basis to compare prosthesis in today's market. Furthermore, this comparative basis is applicable to any type of lower limb prosthesis, i.e. prosthesis for the foot, transfemoral or transtibial amputees.

The devices can be further subdivided on the basis of whether the prosthesis are static (of largely cosmetic value), passive/mechanical (spring loaded or otherwise responsive) or active microprocessor controlled (partly or wholly electronically controlled) prosthesis. Active prosthesis can be further classified by the control strategies employed by them. Not surprisingly, transfemoral (above knee) prosthetics favor actively controlled solutions as stiff knee prosthesis leave everyday activities such as climbing stairs or bending below the waist challenging for amputees. We will briefly overview passive and active solutions for transtibial and transfemoral amputees.

1.1.1.1 Below the Knee prosthetics

The advantage of passive prosthetics are that they are cheap, durable and lightweight. They are also of interest to this study due to their simplicity, which would facilitate their interfacing with our tensegrity system. The first example of below the knee passive prosthetics is the conventional SACH (Solid Ankle Cushion Heel) foot [17] of which prototypes were seen as early as the 1880s, but with concerted development in the late 1950s. The passive SACH foot is the simplest lower limb prosthetic. To perform foot-like functions, rubberized regions bend and deform when weight is transferred from the sound limb onto the prosthetic. This is best suited to low activity users. It also has the advantage of being cheap, water resistant and lightweight. They also provide a dynamic keel, i.e. allowing the forefoot to flex under load, acting as a shock absorber and giving an extra push as the load is removed.

Several other manufacturers are also active in the market, and models with hydraulic or spring loaded systems for more natural gait exist. Among passive prosthetics, they are the most successful in regards to gait quality and patient strain/energy expenditure, even if high performance models can compromise on aesthetics (not appearing as a natural foot cosmetically). Active prosthetic

Figure 1.1: Dynamic Response "J" Foot.

feet have reached remarkable capabilities, including specialized prosthetics designed for sport uses such as running, hiking and rock climbing. Electromyographic signals measured from the residual limb have seen application in such prosthetics as a control signal for the foot position and

Figure 1.2: Vanderbilt prosthetic design.

orientation [18].

1.1.1.2 Above the knee Prosthetics

Though effective mechanical knee types (constant friction, weight-activated stance, polycentric, pneumatic, hydraulic, etc. [19, 4]) are available, which are well suited for walking and standing on even terrain, a transfemoral amputee has to make do without two complex joints, the ankle and the knee, making climbing stairs, standing up from a seated position or other common environments very challenging.

Advanced devices today are beginning to tackle challenging environments such as providing stability while walking downhill, maintaining balance on unstable surfaces, climbing obstacles and other biomimetic functions. These devices perform significantly better in terms of gait quality, however they are still energetically strenuous for users. Researchers from the University of Massachusetts and Vanderbilt University have designed and tested an active prosthesis with powered knee and ankle with pneumatic-type actuators of high actuation potential capable of providing

power output comparable to a natural human leg.

Control strategies were implemented that enables natural, stable interaction between the user and the powered prosthesis [20]. Further developments from the Vanderbilt Center for Intelligent Mechatronics include a control architecture capable of inferring the intent of the user [21], and a prosthetic weighing less than a natural leg that enables users to walk faster and without exhaustion for longer distances. These perform exceptionally in the first and second categories, and are becoming commercially viable in the third category of user aesthetics as well. Most commercially available active prosthesis provide mobile phone applications that enable users to switch between activity modes. Other control strategies include an echo control that tracks the sound limb and effectively mimics its motion with a delay [22]. It should be noted that the higher the level of complexity in the control system, the greater the technical challenges and far greater the demands of the durability and stability tolerance for these highly complex systems.

1.1.2 Common control strategies

The earliest findings were static and mainly of aesthetic nature. Later, body-powered variants were developed to provide the user with more natural control. These prostheses were comparatively cheap and allowed for basic feedback to the controlling muscles but were aesthetically less pleasing than current prostheses. Furthermore, prolonged use applied strain and devices often required unnatural looking movement to control [23]. To overcome those problems, externally powered prostheses were proposed.

This class of devices is divided into switch- controlled and myoelectric prostheses. The switch-based approach involves control similar to the body-powered devices. It allows for a quick learning phase but lacks the feedback that body-powered prostheses provide. Myoelectric devices rely on the electric signals that muscle activity creates [24] There are several control techniques that have been used over time like nut control, robust control (varying velocity and stiffness with time), impedance control and myoelectric control [25].

In most passive-dynamic studies, power comes from the potential energy gained while trajectory based control provides constant actuation to move the system against its natural tendencies

[26]. This work includes trajectory based control actuated by a bunch of strings which are stressed to give the desired shape and stiffness to the structure or to move it to follow a desired path.

1.1.3 Limb-Prosthetic contact

Most of the above knee prosthetics consist of four main parts, socket with a liner, knee, Pylon (lower leg), and feet as shown in figure 1.3. Some include even a shrinker that helps compressing the entire upper limb making it ready for socket fitting and preventing edema.

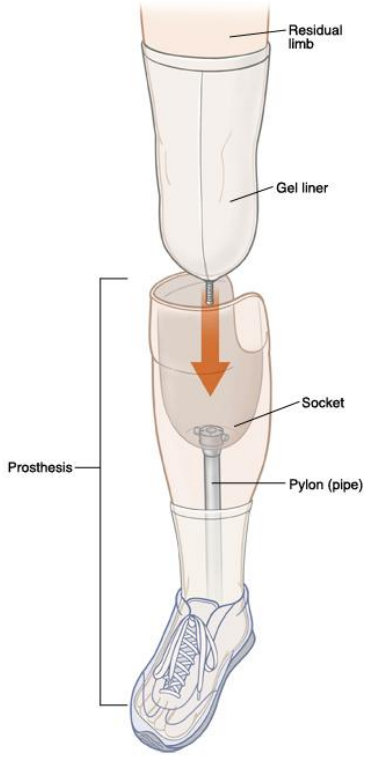

Figure 1.3: Main parts of a prosthetic.
Reprinted from https://www.fairview.org/sitecore/content/Fairview/Home/Patient-Education/Articles/English/l/e/a/r/n/Learning_to_Use_a_Prosthesis_88870

A crucial area of interest for both passive and active prosthetics is the socket-stump interface. Dermatologic conditions are a frequent complication for lower-limb amputees who use a prosthesis [27]. The residual tissues are unaccustomed to bearing loads, leading to acroangiodermatitis, allergic contact dermatitis, infections, ulcerations and other skin diseases [28]. Thus, to cushion

the transfer of load between the residual leg and prosthetic and provide additional suspension of the prosthesis soft prosthetic liners have been developed [29]. Earlier this year, gel based liner systems with 218 embedded electrodes [30] were developed to allow electromyographic control for upper limb prosthesis.

The discussions on the current state-of-the-art sets the context of the field and brings to light areas where tensegrity structure based prosthetics can contribute towards the challenges in design, comfort and control of devices for the growing amputee population. The possible advantages shall be discussed further in the motivations section.

1.1.4 Leg Biomechanics

Bipedal locomotion involves cyclic combinations of flexion and extension of multiple muscles, joint torques and balancing aids like concurrent bending and arm movement. When described in terms of simple mechanics, human gait can be explained by a double pendulum [31]. The major joints that help in the movement of a leg are hip joint, knee and foot joints. The hip flexors, knee extensors and dorsi flexors are for forward propulsion and the hamstring, knee flexors and plantar flexors help in stabilization.

During the normal gait cycle, stance constitutes approximately 60% of the time and 40% of the time is spent in the swing phase [32]. Stance phase is called the support phase where both feet touch the ground, which can be further divided into phases like loading response (0-10%), midstance (10-30%) and terminal stance (30-50%) as shown in figure 1.4 It starts with loading response when the heel makes the first contact and terminates with heel of the support limb swinging away until the heel of the opposite leg makes contact. Swing phase starts with the lift off of a support foot, called as the initial swing (60-70%). It then goes through the mid swing phase (70-85%) and ends with the heel striking the ground again, called as the termination step (85-100%) [31, 23]. There are differing schools of thought regarding the role of ankle push off during the transition phase. Some support the hypothesis that the ankle push-off primarily aids the initiation of leg swing (Meinders et al., 1998; Winter and Robertson, 1978), while others believe its function is to redirect the body's center of mass to provide requisite balance during the step-to-step transition [33].

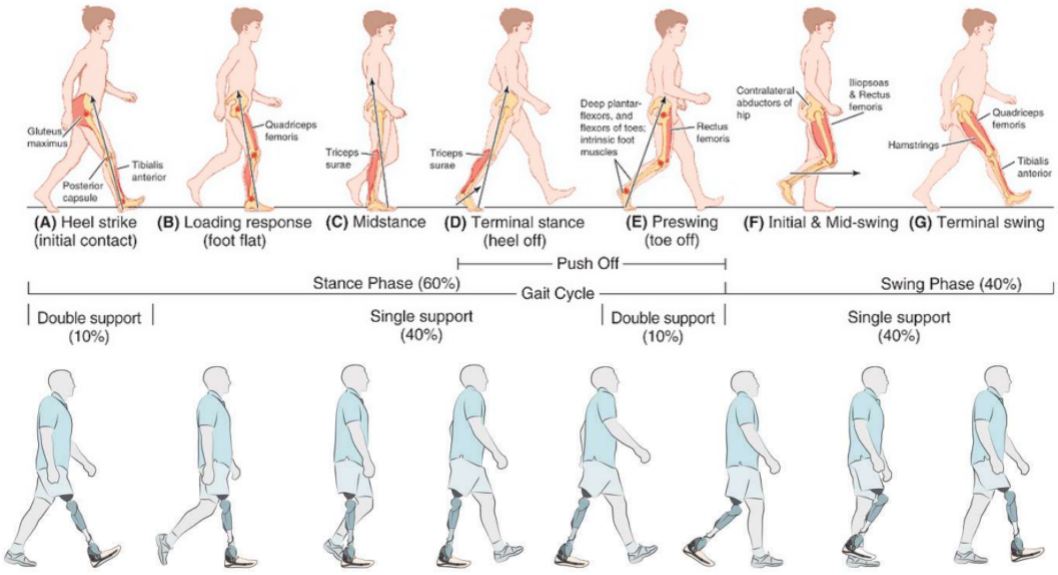

Figure 1.4: Static poses in a gait sequence with and without prosthetic.*

The effective body weight varies depending on the stance and alignment of the weight over the joints space. At the beginning and end of stance, the center of mass drops rapidly toward the floor increasing the ground reaction force to a value greater than the body weight. Whereas, midstance the effective weight directed towards the ground is reduced. Therefore, the composite effect of body weight is determined by measuring the instantaneous ground reaction forces and muscular forces required to stabilize the gait (which vary by both by distribution of weight on each limb and the alignment of body weight over the joints [23]). There is no moment added by the external forces during the swing phase and the muscles counteract any joint moment in that period [31].

Body weight is distributed evenly between the two legs during double support phase in a healthy human but post amputation, it is observed that the center of gravity shifts towards the healthy leg [31].

The understanding of walking dynamics and mechanics of the foot-ground contact is also important, particularly in the design of prosthetic feet. We have in previous sections discussed some

*Reprinted with permission from Biomechanics of Lower Limb Prostheses, by Rajťúková, V. and Michalíková, M. and Bednarčíková, L. and Balogová, A. and Živčák, J., 2014, Procedia Engineering, Volume 96, Page 382-391, Copyright [2014] by Elsevier.

of the progress made in achieving biomimetic function. Although a large number of prosthetic foot types that approach this criteria are commercially available, there are significant gaps in the clinical knowledge regarding the effects of different prosthetic components on various aspects of human mobility e.g. making transfers, maintaining balance, changing walking speed, negotiating ramps and obstacles [34].

1.2 Tensegrity Structures

Tensegrity is a word coined by Buckminster Fuller to describe structures that are made of axially loaded pre-stressed members connecting disjointed compressive members [35]. These structures can be thought of as a network of bar and string members with structural stiffness and rigidity adjusted by a wise choice of network topology and prestress applied in the strings [36]. Tensegrity architecture appears in many biological systems, such as the bone and muscle networks, fibrous structural components in living cells and the molecular structure of spider fiber [36, **?**]. Tensegrity concepts are providing solutions to many structural problems, such as artificial gravity space habitats [37, 38], civil engineering bridges, [39, 40] and impact structures [41]. In addition to those dynamic studies, minimal mass properties of those structural configurations are also analyzed [36, 42]. Recent mathematical results by Skelton show that the minimal mass structure (subject to a stiffness constraint) is a tensegrity structure, for each of the five fundamental problems in engineering mechanics: (i) structures loaded in compression, (ii) structures loaded in tension, (iii) structures loaded in cantilevered bending, (iv) structures loaded in torsion, (v) structures loaded in simply-supported bending.

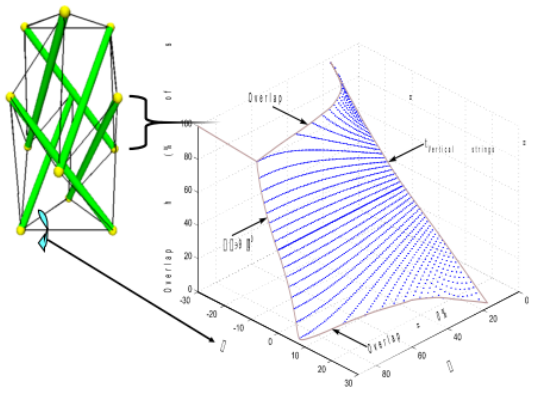

Figure 1.5: Multiple equilibrium paths that can be optimized for desired performance/weight/shape a lower cost of control energy .*

The primary advantage of Tensegrity systems is its ability to efficiently distribute the global stresses to each component of the structure to provide net structural stability throughout the movement with low control energy [43, 44]. It is a unique method in which shape change can be achieved without a change in stiffness as the structure morphs from one equilibrium configuration to another on the control surface [43] as shown in figure 1.5.

1.2.1 Mechanics of Tensegrity Structures

Tensegrity structures are made up of a network of bars and strings arranged in a configuration constrained to some boundary conditions and can be subjected to external loading. If there is only one compressive member connected to a node, the system is called Class 1 Tensegrity System. If k compressive members connect at any node (via a friction-less ball joint), the structure is called Class k Tensegrity System (figure 1.6). The loads in all members are directed axially; strings are only in tension, bars (rods) are only in compression. The absence of bending in each element does allow the bending of overall system even when no individual element bends [43].

*Reprinted with permission from "Tensegrity Systems", by Robert E. Skelton, Mauricio C. de Oliveira, 2009, Springer Nature, Boston, MA. Coyright [2009] Springer-Verlag US.

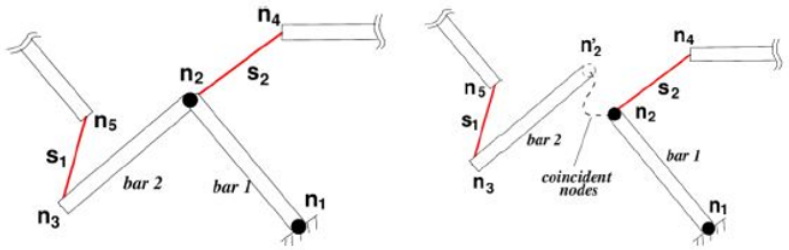

Figure 1.6: Bar to bar connections in a class K tensegrity structure.*

Tensegrity structure is actuated by the elastic force in the strings and the control variable is the rest length of each string [45]. It is this elastic energy in the strings that provides the required stiffness in the structure which may be lost if the strings go slack. This can be quite undesirable especially if too many strings lose tension in the actuation process, the structure is bound to collapse. To provide actuation without loss of stability of the structural system, conditions are posed on the tension of the strings during the actuation process. An alternate way to check for stability of a tensegrity structure can be derived based on positive definiteness of the tangent stiffness matrix, which is the sum of linear and geometrical stiffness matrices [46].

1.2.2 Tensegrity Statics and Dynamics Formulation

In this work, static and dynamic analysis of the tensegrity structure is done with the following assumptions:

1. Strings are massless.

2. Bars are very thin, i.e. the axial moment of inertia is negligible (in comparison to the transverse component).

3. Nodes of the bars for string connections are considered to be exactly at the center of the bar. This ensures zero torque due to the tension in the strings about the center of mass of the bar [43].

*Reprinted with permission from "Tensegrity Systems", by Robert E. Skelton, Mauricio C. de Oliveira, 2009, Springer Nature, Boston, MA. Coyright [2009] Springer-Verlag US.

The terminology of "fixing" the nodes is used frequently in this document which implies that the degree of freedom of that node is zero.

The dynamics for tensegrity systems has been developed by Skelton and the key equations are mentioned here in this section and a more detailed derivation is provided in the Appendix. The readers are directed to [45] should they be interested further in detailed lemmas and their proofs.

Let us first define all the matrices and variables used in the formulation of tensegrity mechanics:

$$
\begin{aligned}
Node\ matrix :& N = [n_1 n_2 n_3 ..... n_{2\beta}], \\
Bar\ matrix :& B = NC_B^T, \\
Bar\ center\ of\ mass\ matrix :& R_b = NC_R^T, \\
String\ matrix :& S = NC_S^T, \\
Tension\ vector :& ||t_i|| = k_i(||s_i|| - s_{0i}) + c_i \frac{s_i^T \dot{s}_i}{||s_i||}, \\
Force\ Density\ vector :& \gamma_i = \frac{||t_i||}{||s_i||}, \\
External\ force\ matrix :& W = [w_1 w_2 w_3 ... w_{2\beta}], \\
F = W - TC_S =& W - NC_S^T \hat{\gamma} C_S.
\end{aligned}
$$

where, N is the matrix with all the nodal coordinates, C_S, C_B and C_R are the connectivity matrices containing (-1,0,1) describing the connection of bars, strings and the center of mass connections in the structure and W is a 3x2β matrix with β being the number of bars and σ being the number of strings.

1.2.2.1 Dynamic Analysis

If we consider a network of bars and strings subjected to some external forces applied at certain nodes defined by matrix, W, we can formulate the dynamics of the tensegrity system using equation 1.1. Using the matrices defined earlier and writing the equations of translational and rotational

motion for each bar in a matrix form for the entire structure, we get:

$$\ddot{N}M + NK = W, \tag{1.1a}$$

$$M = \left[(C_B^T \hat{J} C_B + C_R^T \hat{m} C_R) \right], \tag{1.1b}$$

$$K = \left[C_S^T \hat{\gamma} C_S - C_B^T \hat{\lambda} C_B. \right] \tag{1.1c}$$

1.2.2.2 Static Analysis

We can obtain the equation for static equilibrium condition by putting $\ddot{N}$=0 in the equation 1.1 as given below:

$$\begin{aligned} NK &= W, \\ K &= \left[C_S^T \hat{\gamma} C_S - C_B^T \hat{\lambda} C_B \right], \\ \hat{\lambda} &= -\frac{1}{12} \hat{m}_b \hat{l}^{-2} \lfloor \dot{B}^T \dot{B} \rfloor - \frac{1}{2} \hat{l}^{-2} \lfloor B^T (W - S \hat{\gamma} C_S) C_B^T \rfloor. \end{aligned}$$

The above equation can be formulated as a linear algebra problem, $AX = Y$ where, X is $[\gamma, \lambda]^T$ and A can be written as $[(C_S \otimes I_3)\hat{S},\ \ (-C_B \otimes I_3)\hat{B}]$.

2. MOTIVATION

Tensegrity has the potential to provide minimal mass solution with minimal control effort. With tension in the multitude of strings as the control variable, the tensegrity prosthetic can dynamically mimic the walking/climbing/running motions of a natural leg. This could potentially be achieved with easier control strategies as compared to active prosthesis available today. In general, weight of the prosthetic is directly proportional to the degrees of freedom required, which in turn demands greater strength/control energy. A tensegrity leg, on the other hand, could achieve the same at lower additional weight cost.

Also, nearly 100 percent of trans-tibial amputees experience chronic discomfort at the limb-to-prosthetic interface. One of the reasons is that the residual limb often tends to atrophy, shrinking the stump over time and the prosthetic socket no longer fits as well as when it was designed. However, for tensegrity legs the relative distance between nodes (and consequently the fit) can be controlled by re-configuring the string tensions for the altered shape. If successfully implemented, it might be possible to mass produce a "one-size-fit-all" prosthetic which can readily be configured (in height and width) for any user. Without each user requiring a custom built socket and leg, it could drive costs down significantly.

The design of tensegrity prosthesis would also enhance the development of tensegrity orthotics, i.e. the development of augmentative devices for the physically challenged who do not require amputations. It would also play a role in rehabilitation post injury, as well as in post-operative care and rehabilitation of lower limb amputee patients, acting as a brace/support while they get accustomed to using traditional prosthesis.

Therefore, the aim is to explore the concept of Tensegrity for light and stable artificial legs that can be externally actuated for normal human-like gait in the sagittal plane, on a flat surface. Application of tensegrity systems in prosthesis is a concept currently being explored by certain institutes and manufacturers, but no product has been successfully launched in the market.

This document is divided into three major sections that will follow; Case Study, Results, Sum-

mary and Conclusion. Case Study is further divided into subsections where preliminary design studies and their corresponding static equilibrium analysis is executed, the proposed design of the prosthetic is explained in detail along with its structural and dynamic equilibrium analysis for the two phases of gait and controller design is described for gait simulation.

3.1 Preliminary design studies

Prior to finalizing the design for the prosthetic leg, analytical solutions to some simpler 2D structures were evaluated to get an insight that helps in formulating the design parameters for the final design. All of these structures are put into a class and are named as scissor structures in this document for ease of reference.

3.1.1 For the Symmetric 2D 'X' structure

Let the length of two planar rods $L1 = L2 = L$ and $r1 = r2 = r$

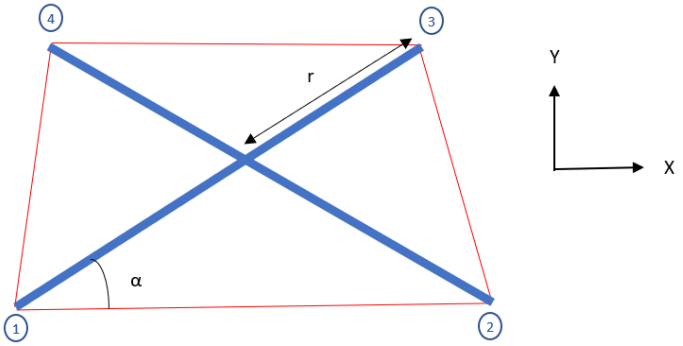

Figure 3.1: 2D Scissor Structure.

where r is shown in figure 3.1. Suppose, the overlap ratio is β

$$\beta = \frac{r}{L} \tag{3.1}$$

Assuming (0,0) divides the two bars in the ratio (r:L) and using, $\frac{L-r}{L} = \frac{1-\beta}{\beta} \sin\alpha = \frac{v}{L-r}$, we have,

$$v = L(1-\beta)\sin\alpha \tag{3.2}$$

since, $\cos\alpha = \frac{h}{L-r}$, we can evaluate the height as,

$$h = L(1-\beta)\cos\alpha \tag{3.3}$$

Using the properties of similar triangles,

$$\frac{v'}{v} = \frac{r}{L-r} = \frac{\beta}{1-\beta} = \frac{h'}{h}$$

$$v' = L\beta\sin\alpha \tag{3.4}$$

$$h' = L\beta\cos\alpha \tag{3.5}$$

Where v, v', h, h' are defined as the y and x coordinates of the bars respectively. Therefore, we can form the Nodes vector matrix and connectivity matrices for the structure as:

$$N = L\left(\begin{Bmatrix} (\beta-1)\cos\alpha & (1-\beta)\cos\alpha & \beta\cos\alpha & -\beta\cos\alpha \\ (\beta-1)\sin\alpha & (\beta-1)\sin\alpha & \beta\sin\alpha & -\beta\sin\alpha \end{Bmatrix}\right) \tag{3.6}$$

$$Cb = \begin{Bmatrix} -1 & 0 & 1 & 0 \\ 0 & -1 & 0 & 1 \end{Bmatrix} \tag{3.7}$$

$$Cs = \begin{Bmatrix} -1 & 1 & 0 & 0 \\ 0 & -1 & 1 & 0 \\ 0 & 0 & -1 & 1 \\ 1 & 0 & 0 & -1 \end{Bmatrix} \tag{3.8}$$

Where N is the node matrix, Cb is bar connectivity matrix and Cs is string connectivity matrix.

using $B = NCb^T$

$$B = L\left(\begin{Bmatrix} \cos\alpha & -\cos\alpha \\ \sin\alpha & \sin\alpha \end{Bmatrix}\right) \tag{3.9}$$

where B is the Bar vectors matrix.

using $S = NCs^T$

$$S = L\left(\begin{Bmatrix} 2(1-\beta)\cos\alpha & (2\beta-1)\cos\alpha & -2\beta\cos\alpha & (2\beta-1)\cos\alpha \\ 0 & \sin\alpha & 0 & -\sin\alpha \end{Bmatrix}\right) \tag{3.10}$$

using $NK = W$ since $\ddot{N} = 0$

$$S\Gamma Cs - B\Lambda Cb = 0 \tag{3.11}$$

where Γ and Λ are diagonal matrices with each diagonal element representing force densities γ_i and λ_j.

Linear algebra problem $AX = b$ is formulated and null space of A is explored, where,

$A = [SCs_i \quad BCb_j]$, $X = \begin{Bmatrix} \gamma_i \\ \lambda_j \end{Bmatrix}$ and $b = W_k$, external force per node

The equilibrium equation was solved for constant $\beta = 0.1$ and varying α. For a zero external force, infinite solutions exist for the problem $AX = 0$ as A has one null space associated with free variable λ_2, the force density in the second bar.

It is observed that the null space does not change for varying alpha while it varies for any change in β. Random values between 5^o and 60^o were chosen to get the normalized null space as:

$$\begin{Bmatrix} 0.0123 \\ 0.0111 \\ 1 \\ 0.111 \\ 0.111 \\ 0.111 \end{Bmatrix}$$

Solving manually, the relations found between the force densities are:

$$\gamma_4 = \lambda_1 = \gamma_2 = \lambda_2, \gamma_3 = \frac{1-\beta}{\beta}\gamma_4, \gamma_1 = \frac{\beta}{1-\beta}\gamma_2 \tag{3.12}$$

3.1.2 For the Symmetric 3D 'X' structure

This subsection extends the 2D structure defined in the previous section into a 3D structure. The 3D structure is formed by connecting the two 2D scissor structures using a common non planar rod. Refer figure 3.2.

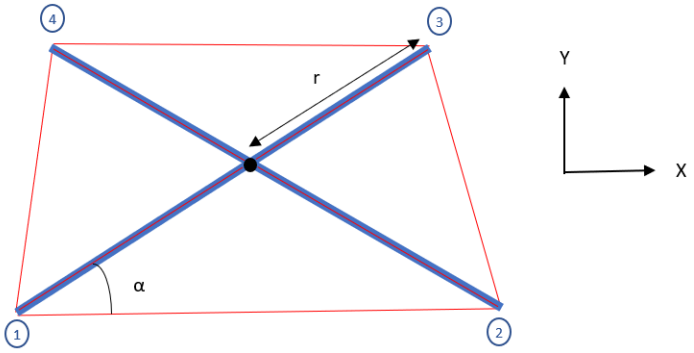

Figure 3.2: 3D Symmetric Scissor Structure.

Length of the two planar rods is L and the length of the non-planar rod is Ls. Variables r, v, v', h, h' and β are same as in the previous section. Therefore, forming the Nodes vector matrix and connectivity matrices for the structure.

$$N = L \left(\begin{Bmatrix} (\beta-1)\cos\alpha & (1-\beta)\cos\alpha & \beta\cos\alpha & -\beta\cos\alpha \\ (\beta-1)\sin\alpha & (\beta-1)\sin\alpha & \beta\sin\alpha & -\beta\sin\alpha \\ -\frac{Ls}{2L} & -\frac{Ls}{2L} & -\frac{Ls}{2L} & -\frac{Ls}{2L} \end{Bmatrix} \right) \tag{3.13}$$

$$N' = L\left(\begin{Bmatrix} (\beta-1)\cos\alpha & (1-\beta)\cos\alpha & \beta\cos\alpha & -\beta\cos\alpha \\ (\beta-1)\sin\alpha & (\beta-1)\sin\alpha & \beta\sin\alpha & -\beta\sin\alpha \\ \frac{Ls}{2L} & \frac{Ls}{2L} & \frac{Ls}{2L} & \frac{Ls}{2L} \end{Bmatrix}\right) \tag{3.14}$$

$$Nv = \begin{Bmatrix} 0 & 0 \\ -Ls & Ls \end{Bmatrix} \tag{3.15}$$

Where, N, N', Nv are the node matrices for the first structure, second scissor structure and the non planar rod respectively. Therefore, Node matrix for the entire 3D structure can be expressed as below:

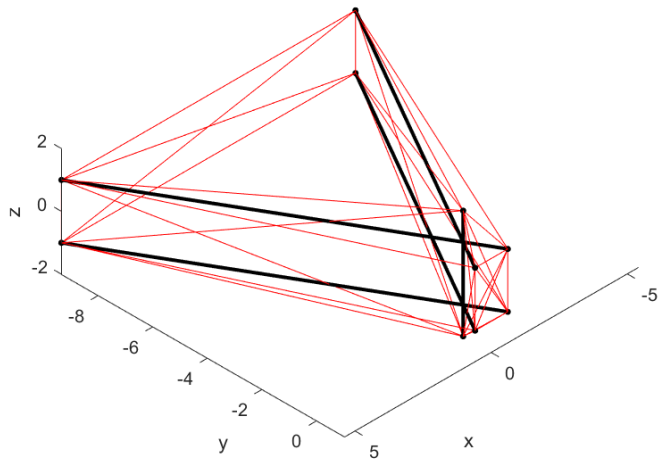

Figure 3.3: 3D Symmetric Scissor Tensegrity Structure.

$$Nstr = \begin{Bmatrix} N & Nv & N' \end{Bmatrix} \tag{3.16}$$

$$Cbstr = \begin{Bmatrix} Cb & 0_{2\times 6} \\ Cbo & 0_{2\times 4} \\ 0_{2\times 6} & Cb \end{Bmatrix} \tag{3.17}$$

Where, $Cbstr$ is the bar connectivity matrix. Cb is defined in Section 1.

$Cb_o = \begin{Bmatrix} 0 & 0 & 0 & 0 & -1 & 1 \end{Bmatrix}$.

The string connectivity matrix is broken down into two sections. One is the strings connecting nodes of the respective scissor structures and the second consists of the coupling strings between the two scissors.

$$Cs_{coupling} = \begin{Bmatrix} -1 & 0 & 0 & 0 & 0 & 0 & 1 & 0 & 0 & 0 & 0 & 0 \\ 0 & -1 & 0 & 0 & 0 & 0 & 0 & 1 & 0 & 0 & 0 & 0 \\ 0 & 0 & 0 & -1 & 0 & 0 & 0 & 0 & 0 & 1 & 0 & 0 \\ 0 & 0 & -1 & 0 & 0 & 0 & 0 & 0 & 0 & 1 & 0 & 0 \\ 0 & -1 & 0 & 0 & 0 & 0 & 1 & 0 & 0 & 0 & 0 & 0 \\ 0 & 0 & -1 & 0 & 0 & 0 & 0 & 0 & 0 & 1 & 0 & 0 \\ 0 & 0 & 0 & -1 & 0 & 0 & 0 & 0 & 1 & 0 & 0 & 0 \end{Bmatrix}$$

$$Cs_{str} = Cs + \left(\begin{Bmatrix} 0_{24\times 10} \\ Cs_{coupling} \end{Bmatrix} \right) \tag{3.18}$$

Where Cs_{str} is string connectivity matrix for the structure and $Cs_{coupling}$ defines the coupling strings connectivity.

using $NK = W$ since $\ddot{N} = 0$

$$S_{str}\, \Gamma\, Cs_{str} - B_{str}\, \Lambda\, Cb_{str} = 0 \tag{3.19}$$

where B_{str} and S_{str} are calculated using $B = N_{str} Cbstr^T$ and $S = N_{str} Cs_{str}^T$.

The equilibrium equation was solved for constant $\beta = 0.1$ and varying α. For a zero external force, infinite solutions exist for the problem $AX = 0$ as A has 13 null spaces associated with free

variables γ_{24}, γ_{25}, γ_{26}, γ_{27}, γ_{28}, γ_{30}, γ_{31}, γ_{32}, λ_1, λ_2, λ_3, λ_4, λ_5.

The null space did not change for the varying alpha (the angle between two planar bars). 'α' is picked to be any random value between 5^o and 60^o as shown in figure 3.4. The null space changes for different values of β.

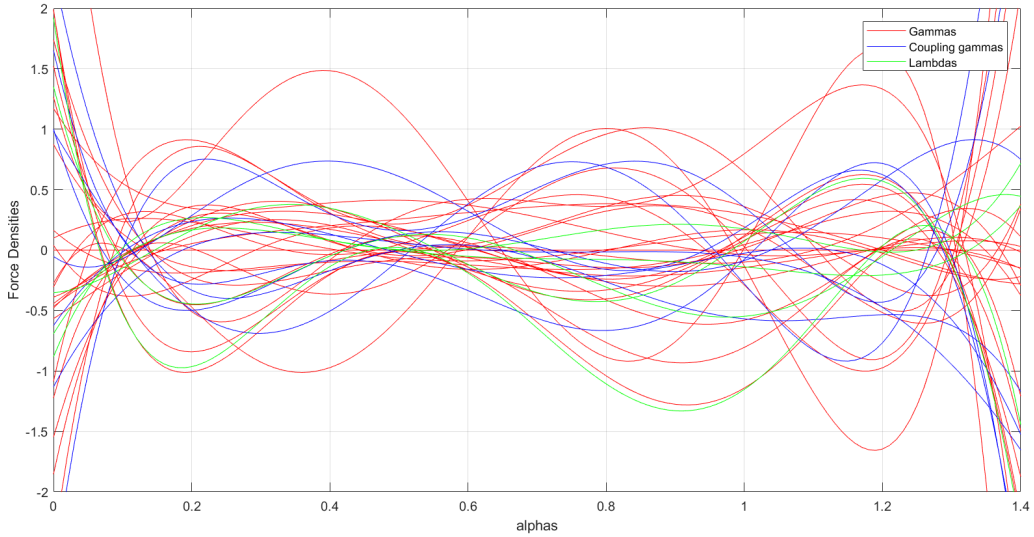

Figure 3.4: Force densities in bars and strings for symmetric 3D scissor structure.

3.1.3 Asymmetric 3D Scissor structure

The length of two planar rods $L1 = L2 = L$ and the overlap ratio

$$\beta_1 = \frac{r_1}{L},\ \beta_2 = \frac{r_2}{L} \tag{3.20}$$

where $r1$, $r2$ are shown in figure 3.6.

If the rods intersect at (0,0), using the section formula $\frac{x_1 r_1 + x_3(L-r_1)}{L} = 0$

$$x_3 = (\frac{\beta_1}{(\beta_1 - 1)})x_1 \tag{3.21}$$

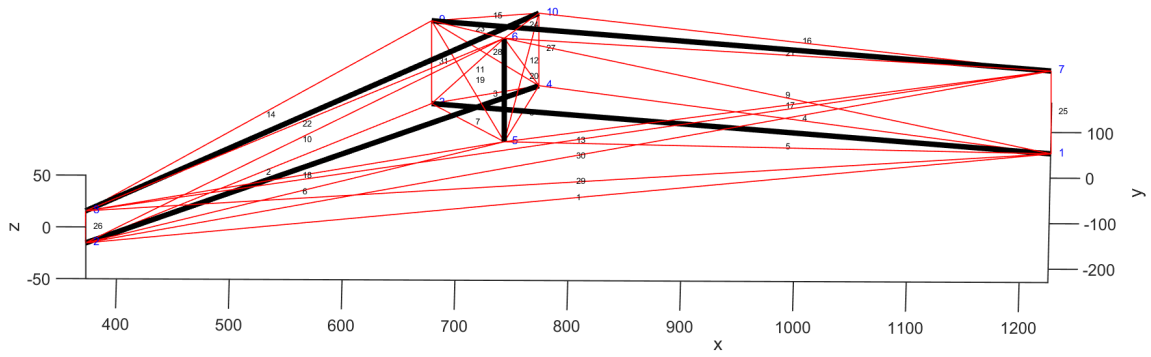

Figure 3.5: View 1 of Tensegrity Prosthetic with strings numbered

Similarly,

$$y_3 = (\frac{\beta_1}{(\beta_1 - 1)})y_1,\ x_4 = (\frac{\beta_2}{(\beta_2 - 1)})x_2,\ y_4 = (\frac{\beta_2}{(\beta_2 - 1)})y_2 \tag{3.22}$$

Let ϕ and ϕ' be the angles that the first and second bars make with the x-axis respectively. α is the angle between two planar bars as shown in figure 3.6.

$$\tan\phi = \frac{y_3 - y_1}{x_3 - x_1}$$

$$\phi' = pi - (\phi + \alpha)$$

$$y_4 = -\tan\phi' x_4, y_2 = -\tan\phi' x_2 \tag{3.23}$$

Also, we know,

$$(x_4 - x_2)^2 + (y_4 - y_2)^2 = L^2$$

this leads to

$$x_2^2 = \frac{L^2(\beta_2 - 1)^2}{\sec^2\phi'} \tag{3.24}$$

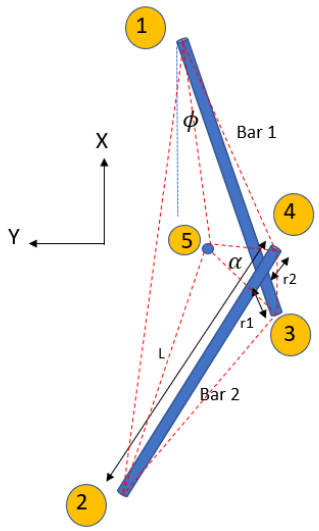

Figure 3.6: 3D Asymmetric Scissor Structure.

Coordinates of the non coplanar bar is computed using the previously calculated coordinates.

$$x_5 = \frac{x_1 + x_2}{2}, y_5 = (\frac{y_1 + y_2}{2})$$

Therefore, node coordinates matrix for one asymmetric scissor structure defined by inputs of $\beta_1, \beta_2, \alpha, \psi, x_1$ is

$$N = \begin{Bmatrix} x_1 & L(\beta_2 - 1)\cos\phi' & \frac{\beta_1}{\beta_1 - 1}x_1 & \beta_2 L\cos\phi' \\ \sqrt{|(L^2((1-\beta_1)^2) - x_1^2))|} & L(\beta_2 - 1)\sin\phi' & \frac{\beta_1}{\beta_1 - 1}y_1 & \beta_2 L\sin\phi' \\ \frac{-Ls}{2} & \frac{-Ls}{2} & \frac{-Ls}{2} & \frac{-Ls}{2} \end{Bmatrix}$$

$$N' = \begin{Bmatrix} x_1 & L(\beta_2 - 1)\cos\phi' & \frac{\beta_1}{\beta_1 - 1}x_1 & \beta_2 L\cos\phi' \\ \sqrt{|(L^2((1-\beta_1)^2) - x_1^2))|} & L(\beta_2 - 1)\sin\phi' & \frac{\beta_1}{\beta_1 - 1}y_1 & \beta_2 L\sin\phi' \\ \frac{Ls}{2} & \frac{Ls}{2} & \frac{Ls}{2} & \frac{Ls}{2} \end{Bmatrix}$$

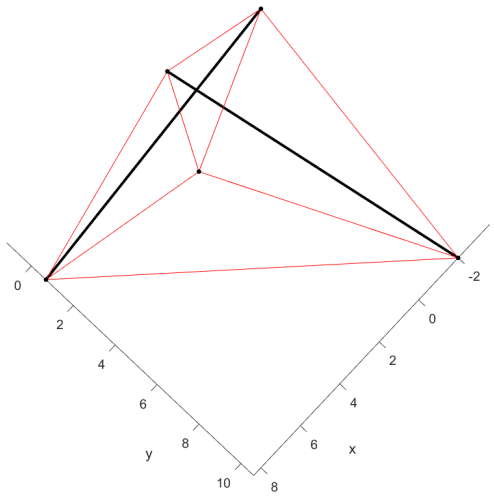

Figure 3.7: View 2 of Tensegrity Prosthetic with initial string configuration.

$$Nv = \begin{Bmatrix} x_5 & x_5 \\ y_5 & y_5 \\ \frac{-Ls}{2} & \frac{Ls}{2} \end{Bmatrix}$$

$$N_{str} = \begin{Bmatrix} N & Nv & N' \end{Bmatrix}$$

3.2 Gait Formulation

Gait is modeled separately as per its two phases i.e. Stance phase and Swing phase. Simulation is run for one gait cycle where the cycle initiates with the stance phase followed by the transition phase and then swing for just one leg. Transition phase encapsulates the three sub-phases (terminal stance, double support and pre-swing) that occur when the leg moves from stance phase to the swing phase. Different poses of the leg during one gait cycle are configured using the hip angle (ϕ) and knee angle (α). The anthropometric characteristics of the individual used for modeling gait are listed in table 3.1 and the parameters of the modeled gait cycle are listed in table 3.2.

*Transition time denotes the time taken to obtain the transition from stance phase to swing phase which includes time for double support, pre-swing time and terminal stance.

Weight of the individual(W_t)	600 kgf
Mass of the lower leg+foot	6.05 % of W_t
Length of the leg	550mm
Length of the thigh	250mm
Knee dimensions	75mm $\times$ 50mm

Table 3.1: Individual's Anthropometrics.

Gait Speed	10 sec per gait cycle
Step length	660mm
Swing time	4 sec
Stance time	5.95 sec
Transition time *	0.05sec

Table 3.2: Gait Cycle Parameters.

Swing phase can be approximately modeled after a damped double pendulum as shown in the figure 3.11 while the stance phase can be modeled using a damped inverted pendulum as shown in figure 3.12. As the foot is not modeled in the design, the transition phase is modeled using static analysis for the series of poses defined by a range of hip (ϕ) and knee angles (α) selected for the transition time. The details regarding dynamics, boundary conditions and design parameter

Phase	Initial phi	Initial alpha	Final Phi	Final alpha
Stance	33^o	7.9^o	-3.5^o	33.8^o
Swing	-0.67^o	40.6^o	32^o	7^o
Transition	-3.64^o	34.47^o	-0.65^o	40.5^o

Table 3.3: Initial Hip and knee angles to configure the three gait phases; Stance, Swing and Transition.

selection associated with each phase are elaborated in the following sections. Strings in the subsequent sections are called active and passive depending on whether they are actively actuated by the controller in a particular phase. Different sets of strings are active or passive in different phases

depending on the boundary conditions. These redundant strings can be pre-stressed for additional set of optimal gammas to stabilize the pose and to avoid slack in the strings.

3.2.1 Non-linear least squares Curve Fitting

A mathematical procedure for finding the best-fitting curve to a given set of points is by minimizing the sum of the squares of the offsets ("the residuals") of the points from the curve. The logic behind using the the sum of the squares of the offsets in place of the offset absolute values is to allow the residuals to be treated as a continuous differentiable quantity. This however can lead to a disproportionate effect on the fit due to outliers.

3.2.1.1 Linear Least Squares

Gauss's linear least squares fitting technique is the simplest and most commonly applied form of linear regression for finding the optimum choice for unknown parameters to solve for an estimated $\hat{x}$ that minimizes the residual error, e [47]. If we have a measurement equation of the form

$$y = a_0 x_0 + a_1 x_1 + ...a_m x_m + e$$

, we can write this in vector form as

$$\mathbf{Y} = H\mathbf{X} + \mathbf{E}$$

where $\mathbf{E}$ is a vector comprising of the measurement error and $\hat{\mathbf{X}}$ are the estimated values for $\mathbf{X}$. The cost function thus becomes :

$$J = \frac{1}{2}\mathbf{E}^T\mathbf{E}$$

which can be written as,

$$J = \frac{1}{2}(\mathbf{Y}^T\mathbf{Y} - 2\mathbf{Y}^T H\hat{\mathbf{X}} + \hat{\mathbf{X}}H^T H\hat{\mathbf{X}})$$

Using the necessary conditions of optimality from variational calculus, we get

$$\hat{\mathbf{X}} = (H^T H)^{-1} H^T \mathbf{Y} \tag{3.25}$$

The above approach assumed equal weights for the least square fitting which may not be ideal since the measurements are not generally made with equal precision. In such cases, a positive definite weighting matrix, W, is used to get a better fit of the data. After incorporating the weighting matrix in the equation 3.25, we get

$$\hat{\mathbf{X}} = (H^T W H)^{-1} H^T W \mathbf{Y} \tag{3.26}$$

Nonlinear least squares fitting is often times achieved by iteratively applying linear least squares to a linearized form of the function until convergence is achieved [47]. Non-linear least square curve fitting is also done using certain basis functions.

3.2.1.2 Fourier approximation

Fourier approximation uses least square estimation while utilizing orthogonal basis functions. A Fourier series is a harmonic expansion of sines and cosines expressed as:

$$y(t) = a_0 + \sum_{n=1}^{\infty} a_n \cos(n\omega t) + \sum_{n=1}^{\infty} b_n \sin(n\omega t) \tag{3.27}$$

On multiplying the above equation with $\cos(\omega t)$ and integrating from 0 to T where T is the final time, we get

$$\int_0^T y(t)\cos(\omega t)dt = a_0 \int_0^T \cos(\omega t)dt + a_1 \int_0^T (\cos(\omega t))^2 dt + ... + b_1 \int_0^T y(t)\cos(\omega t)\sin(\omega t)dt + ... \tag{3.28}$$

Since, sines and cosines are mutually orthogonal, every integral on the right side of the equation 3.28 is zero except the $(\cos(\omega t))^2$ term. Therefore,

$$a_1 = \frac{\int_0^T y(t)\cos(\omega t)dt}{\int_0^T (\cos(\omega t))^2 dt} \tag{3.29}$$

Similarly, all the coefficients can be computed as

$$a_n = \frac{2}{T}\int_0^T y(t)\cos(n\omega t)dt \tag{3.30a}$$

$$b_n = \frac{2}{T}\int_0^T y(t)\sin(n\omega t)dt \tag{3.30b}$$

where n defines the order of Fourier functions chosen for data fitting. Care must be taken about keeping number of data points used for the curve fitting greater than $(n+1)$.

3.2.1.3 Evolution of Hip and knee angles

The evolution of knee and hip angles are usually obtained by taking images of a healthy subject fitted with photo-sensitive markers. The pose of the individual is obtained by using chain kinematics with the help of the change in the relative positions of the markers and the velocity of the subject. This data is available in some of the standard libraries or is made available by some of the authors in their journals. In this work, this data is taken from [48] and is fitted using upto 8^{th} order Fourier series by least square approximations to obtain a curve shown in figure 3.8. The coefficients of the fourier functions are listed in the table 3.4. The coefficients of the functions used to approximate the data on hip and knee angles for both stance and swing are given in the table 3.4.

These expressions are derived as a function of gait cycle percentage and are fed into tensegrity dynamics to calculate the reaction forces and eventually control the proposed prosthetic tensegrity structure to generate an approximation to human gait.

3.2.2 Evolution of Ground reaction forces

The Vertical Ground reaction force data is taken from the table data given in [48]. The data is fitted into a polynomial function such that it matches the given ground reaction profile following the least square estimation using fourier functions explained in section 3.2.1 .

Parameter	Swingϕ	Swing α	Stanceϕ	Stance α	VGRF	LGRF
w	0.9335	0.8518	0.7199	0.7168	0.7583	0.8102
a0	17.52	20.45	14.3	22.55	0.09657	0.6114
a1	-18.26	13.56	21.28	5.329	0.08528	-0.4508
b1	9.506	35.64	3.186	-16.7	-0.07396	0.3309
a2	-1.832	4.667	-0.05438	-13.5	0.01786	-0.06295
b2	5.252	12.51	-4.072	-2.341	-0.118	0.4438
a3	2.149	4.354	-1.998	-5.442	-0.06537	0.08095
b3	-0.02299	-6.853	-0.2706	4.067	-0.09295	0.04492
a4	-0.4205	-2.942	-0.522	-0.5265	-0.07765	0.01994
b4	-0.4152	0.102	0.722	2.393	-0.02274	-0.02835
a5	-0.03795	0.0546	0.02918	0.04408	-0.04473	-
b5	0.09035	0.3735	0.2689	0.3513	0.01149	-
a6	-	-	-	-	-0.01487	-
b6	-	-	-	-	0.01607	-
a7	-	-	-	-	-6.278e-05	-
b7	-	-	-	-	0.01027	-
a8	-	-	-	-	0.003786	-
b8	-	-	-	-	0.002035	-

Table 3.4: Fourier parameters for leg angles and external forces.

3.2.3 Dynamics of Swing and Stance via damped pendulum mechanics

The following sub-sections describe the equivalent kinematics and dynamics of the stance and swing phase of the gait using a damped double pendulum and inverted double pendulum respectively.

3.2.3.1 Swing Phase Dynamics

Assuming [$\tilde{e}_1$,$\tilde{e}_2$] is the frame moving at a constant velocity with respect to the inertial frame.

$$\mathbf{r}_1 = 0$$

$$\mathbf{r}_2 = -l\cos\phi\tilde{\mathbf{e}}_\mathbf{2} + l\sin\phi\tilde{\mathbf{e}}_\mathbf{1}$$

$$\mathbf{r}_3 = -l\cos\phi\tilde{\mathbf{e}}_\mathbf{2} + l\sin\phi\tilde{\mathbf{e}}_\mathbf{1}$$

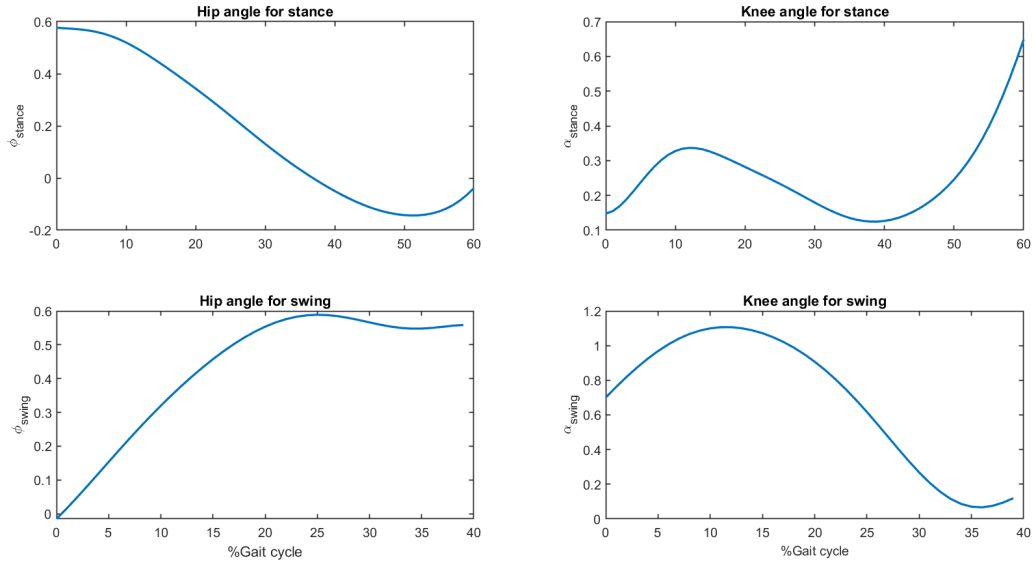

Figure 3.8: Evolution of ϕ and α for the respective gait cycles.

$$V = m_1 g(0) - m_2 g l \cos\phi - m_3 g(l\cos\phi + l\cos\alpha) \tag{3.31}$$

$$\dot{\mathbf{r}}_\mathbf{2} = \dot{\phi}(l\cos\phi)\tilde{\mathbf{e}}_\mathbf{1} + l\sin\phi\tilde{\mathbf{e}}_\mathbf{2}$$

$$\dot{\mathbf{r}}_\mathbf{3} = (\dot{\phi}(l\cos\phi) + \dot{\alpha}(l\cos\alpha))\tilde{\mathbf{e}}_\mathbf{1} + (\dot{\phi}(l\sin\phi) + \dot{\alpha}(l\sin\alpha))\tilde{\mathbf{e}}_\mathbf{2}$$

$$\begin{aligned} T &= \frac{1}{2}m_1\dot{\mathbf{r}}_\mathbf{1}^2 + \frac{1}{2}m_2\dot{\mathbf{r}}_\mathbf{2}^2 + \frac{1}{2}m_3\dot{\mathbf{r}}_\mathbf{3}^2, \\ T &= \frac{1}{2}(m_2+m_3)\dot{\phi}^2 l^2 + \frac{1}{2}m_3\dot{\alpha}^2 l^2 + m_3 l^2\dot{\phi}\dot{\alpha}\cos(\phi-\alpha) \end{aligned} \tag{3.32}$$

Evaluating Lagrangian by $L = T - V$,

$$L = \frac{1}{2}(m_2+m_3)\dot{\phi}^2 l^2 + \frac{1}{2}m_3\dot{\alpha}^2 l^2 + m_3 l^2\dot{\phi}\dot{\alpha}\cos(\phi-\alpha) + (m_2+m_3)gl\cos\phi + m_3 gl\cos\alpha \tag{3.33}$$

$$\begin{aligned} \frac{d}{dt}\frac{\partial L}{\partial\dot{\phi}} - \frac{\partial L}{\partial\phi} &= -c1\dot{\phi} \\ \frac{d}{dt}\frac{\partial L}{\partial\dot{\alpha}} - \frac{\partial L}{\partial\alpha} &= -c2\dot{\alpha} \end{aligned} \tag{3.34}$$

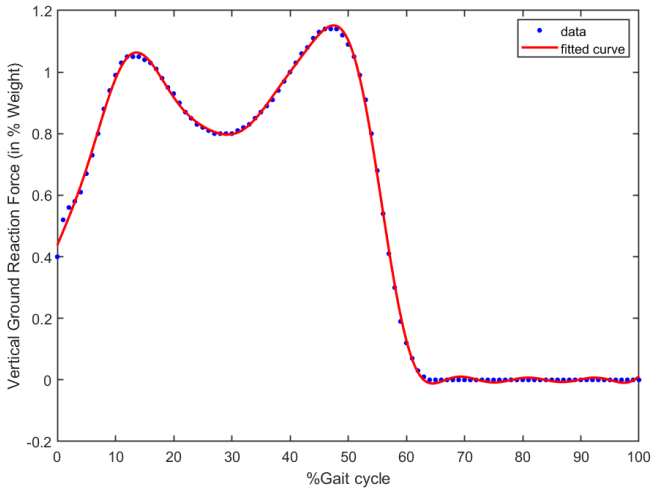

Figure 3.9: Fitted Vertical ground reaction force curve.

$$(m_2+m_3)l^2\ddot{\phi}+m_3l^2\ddot{\alpha}\cos(\phi-\alpha)+(m_2+m_3)gl\sin\phi+m_3l^2\dot{\alpha}^2\sin(\phi-\alpha)=-c1\dot{\phi} \quad (3.35)$$

$$m_3l^2\ddot{\alpha}+m_3l^2\ddot{\phi}\cos(\phi-\alpha)+m_3gl\sin\alpha-m_3l^2\dot{\phi}^2\sin(\phi-\alpha)=-c2\dot{\alpha} \quad (3.36)$$

$$\ddot{\phi}_w=\frac{-m_3l^2\ddot{\alpha}_w\cos(\phi_w-\alpha_w)-(m_2+m_3)gl\sin\phi_w-m_3l^2\dot{\alpha}_w^2\sin(\phi_w-\alpha_w)+c_1\dot{\phi}_w}{(m_2+m_3)l^2} \quad (3.37)$$

$$\ddot{\alpha}_w=\frac{-m_3l^2\ddot{\phi}_w\cos(\phi_w-\alpha_w)-m_3gl\sin\alpha_w+m_3l^2\dot{\phi}_w^2\sin(\phi_w-\alpha_w)+c_2\dot{\alpha}_w}{m_3l^2} \quad (3.38)$$

3.2.3.2 Stance Phase Dynamics

Stance phase can be modeled as a damped inverted pendulum with external forces like the weight of the individual and friction.

$$V=m_1g(0)-m_2gl\cos\phi-m_3g(l\cos\phi+l\cos\alpha) \quad (3.39)$$

$$\dot{\mathbf{r}}_\mathbf{2}=\dot{\phi}(l\cos\phi)\tilde{\mathbf{e}}_\mathbf{1}+l\sin\phi\tilde{\mathbf{e}}_\mathbf{2}$$

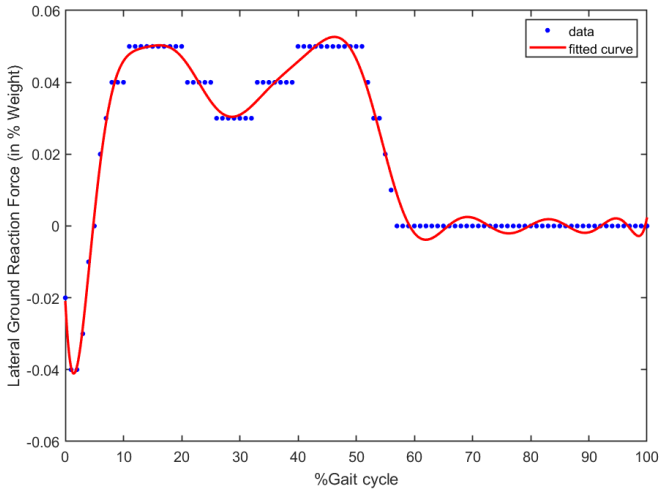

Figure 3.10: Fitted Lateral ground reaction force curve.

$$\dot{\mathbf{r}}_\mathbf{3} = (\dot{\phi}(l\cos\phi) + \dot{\alpha}(l\cos\alpha))\tilde{\mathbf{e}}_\mathbf{1} + (\dot{\phi}(l\sin\phi) + \dot{\alpha}(l\sin\alpha))\tilde{\mathbf{e}}_\mathbf{2}$$

$$L = \frac{1}{2}(m_1+m_2)\dot{\alpha}^2 l^2 + \frac{1}{2}m_1\dot{\phi}^2 l^2 + m_1 l^2\dot{\phi}\dot{\alpha}\cos(\phi-\alpha) - (m_1+m_2)gl\cos\alpha - m_1 gl\cos\phi \quad (3.40)$$

$$\begin{aligned} \frac{d}{dt}\frac{\partial L}{\partial\dot{\phi}} - \frac{\partial L}{\partial\phi} &= -d1\dot{\phi} \\ \frac{d}{dt}\frac{\partial L}{\partial\dot{\alpha}} - \frac{\partial L}{\partial\alpha} &= -d2\dot{\alpha} \end{aligned} \quad (3.41)$$

$$\ddot{\alpha}_t = \frac{-m_2 l^2\ddot{\phi}_t\cos(\phi_t-\alpha_t) + (m_1+m_2)gl\sin\alpha_t - m_2 l^2\dot{\phi}_t^2\sin(\phi_t-\alpha_t) + d_1\dot{\alpha}_t}{(m_1+m_2)l^2} \quad (3.42)$$

$$\ddot{\phi}_t = \frac{-m_2 l^2\ddot{\alpha}_t\cos(\phi_t-\alpha_t) - m_2 gl\sin\phi_t + m_2 l^2\dot{\alpha}_t^2\sin(\phi_t-\alpha_t) + d_2\dot{\phi}_t}{m_2 l^2} \quad (3.43)$$

where ϕ_w and α_w are angles that hip and knee make with $\tilde{\mathrm{e}}_2$ respectively in the swing phase. Similarly, ϕ_t and α_t are hip and knee angles for the stance phase. m_1, m_2 and m_3 are the masses of hip, knee and foot respectively. $c1$, $c2$, $d1$ and $d2$ are the torsional damping coefficients.

Post balancing the force and torque acting on the system in both the phases, the following relations are derived.

$$R_w = R_1\tilde{\mathbf{e}}_\mathbf{1} + R_2\tilde{\mathbf{e}}_\mathbf{2}$$

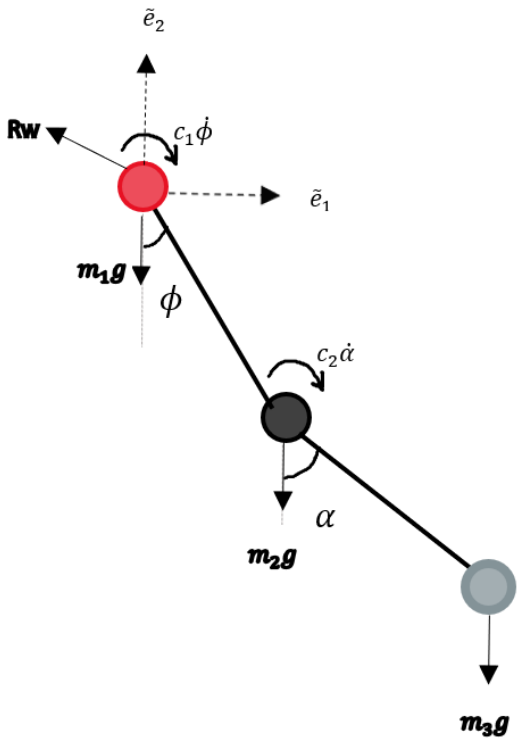

Figure 3.11: Swing Phase modeled as double pendulum.

$$
\begin{aligned}
R_1 &= -m_2 g \sin(\alpha_w) - m_3 g(\sin(\alpha_w) + \sin(\phi_w)) + c_1\dot{\phi_w} + c_2\dot{\alpha_w} \\
R_2 &= (m_1 + m_2 + m_3)g
\end{aligned}
\tag{3.44}
$$

$$R_t = Rf_1\tilde{\mathbf{e}}_\mathbf{1} + Rf_2\tilde{\mathbf{e}}_\mathbf{2}$$

$$
\begin{aligned}
Rf_1 &= W_t + m_1 g(\sin(\alpha_t) + \sin(\phi_t)) + m_2 g \sin(\alpha_t) + d_1\dot{\alpha_t} + d_2\dot{\phi_t} \\
Rf_2 &= (m_1 + m_2 + m_3)g
\end{aligned}
\tag{3.45}
$$

Where R_w and R_t are reaction forces in the swing and stance phases respectively and W_t is the weight of the individual.

3.3 ProTense Design Scheme

The prosthetic leg consists of 5 bars with 2 bars (Bar 1 and Bar 3) being strapped to the thigh of the individual and the other two (Bar 2 and Bar 5) represent the lower leg. One bar (Bar 3) is placed at the back of the knee on which the leg is cradled. The schematic is shown in figure 3.13

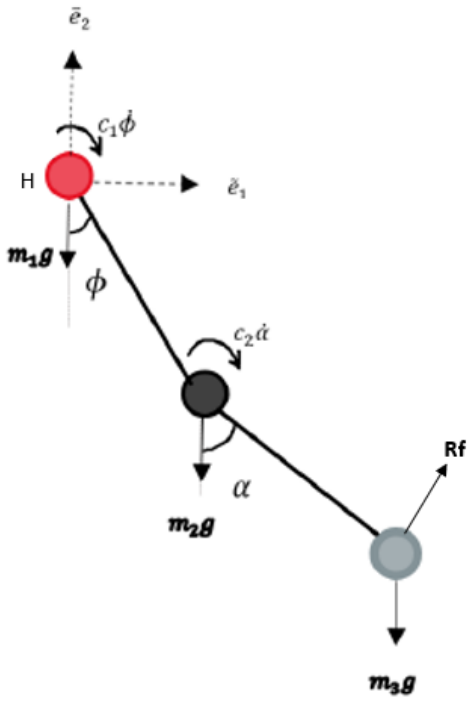

Figure 3.12: Stance Phase modeled as inverted double pendulum.

where it can be observed that Bar 3 is aligned with the z-axis.

There are two concepts on which the prosthetic leg is modeled. The first design (ProTense Design A) assumes that the knee amputee has healthy hip muscles and is controlled according to the inputs received from the hip. The second design (ProTense Design B) is built for the individuals who need additional support for the movement of the upper leg owing to weak hip/thigh muscles. The boundary conditions, string configuration and the actuator energy are different for both the design approaches, Design A (section 3.4) and Design B (section 3.5).

3.3.1 ProTense Fitting

ProTense can be visualized as two bars strapped on the sides of a thigh of an individual with the help of Velcro and two bars strapped to the lower leg if present (see figure 3.15). The motors that pull the strings will be attached to the individual's lower torso. The weight of the entire structure

Figure 3.13: Protense Design A View 1.

Figure 3.14: Design A (left) B (right).

with motors and electronics is not calculated but the structure weighs approximately 1kg. The individual will wear a thin sleeve over which the bars will be placed to minimize the build up of uncomfortable stress on the skin. The fifth bar is placed such that it presses against the lower half of the upper thigh in case of an above knee amputee. For Design B, there are two strings emanating from each side of the hip to support the prosthetic structure as shown in figure 3.14. The string nodes are attached to the lower most area of the torso.

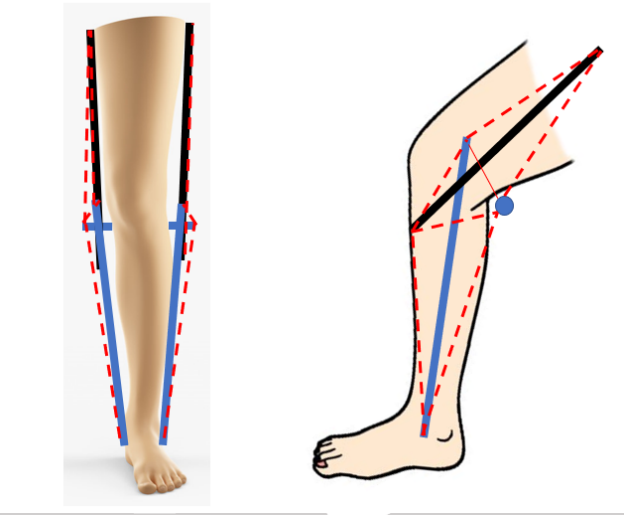

Figure 3.15: A demonstration of ProTense Design A fitting.

3.3.2 Coordinate System

Different schemes for finding the coordinates of the nodes in the inertial frame are formulated for stance and swing to mimic the motion of a leg while walking. We begin the simulation at the start of the stance phase where the initial foot coordinates in the inertial frame are user provided. The foot remains planted on the ground in the stance phase and the position of the foot at the end of stance is fed to model the transition phase i.e. End stance, double support and pre-swing. Since ankle is not modeled in the design, the foot coordinates are assumed to remain constant during the transition phase. The scheme of coordinate system is the same for both stance and transition phases.

3.3.2.1 Stance Phase

Keeping in mind figure 3.6, the overlap ratio of the two bars can be denoted by variables, $\beta_1 = \frac{r_1}{L}$ $\beta_2 = \frac{r_2}{L}$.

$$x2 = L\cos\psi(\beta_2 - 1)\cos\theta \tag{3.46}$$

where ψ is the angle that bar 2 makes with the x-axis in x-z plane. since bar 2 makes an angle θ with the x-axis,

$$y_4 - y_2 = (x_4 - x_2)\tan\theta$$

On substituting the above equation in the length constraint equation and simplifying,

$$(x_4 - x_2)^2 + (y_4 - y_2)^2 = L^2\cos^2\psi$$

we get, $x_4 = x_2 + L\cos\phi\cos\psi$ and $y_4 = (x_4 - x_2)\tan\theta + y_2$. If bar 1 and bar 2 projected on x-y plane intersect at xi and yi, we can use the section formula to write,

$$xi = (1 - \beta_2)x_4 + \beta_2 x_2$$

$$yi = (1 - \beta_2)y_4 + \beta_2 y_2$$

On applying the section formula for bar 1, x_1 and x_3 can be written as,

$$x_3 = xi - \beta_1 L\cos(\phi)$$

$$x_1 = \frac{xi - (1 - \beta_1)x_3}{\beta_1}$$

Since bar 1 makes an angle ϕ with the x-axis,

$$y_3 = yi + \beta_1\tan(\phi)(x_3 - x_1)$$

$$y_1 = \frac{yi - (1 - \beta_1)y_3}{\beta_1}$$

$$x_5 = xi - a_x$$

$$y_5 = yi - a_y$$

$$z_4 = -0.35L_s$$

$$z_2 = z_4 + L\sin\psi$$

where a_x and a_y are design parameters that vary for different phases and gait cycle percentage.

3.3.2.2 Swing Phase

Taking the hip nodes (x_1, y_1) obtained at the end of the stance phase as the initial position of the hip in the swing phase. Assuming bar 1 makes an angle ϕ and bar 2 makes an angle of θ with the x axis, the coordinates of bar 1 can be computed as follows,

$$x_3 = x_1 - L\cos\phi$$

$$y_3 = y_1 + \tan\phi$$

$$(x_1)^2 + (y_1)^2 = L^2(1-\beta_1)^2$$

$$y_1 = x_1\tan\phi$$

which leads to

$$x_1 = L(1-\beta_1)\cos\phi$$

$$y_3 = (\frac{\beta_1}{(\beta_1 - 1)})y_1$$

$$x_3 = (\frac{\beta_1}{(\beta_1 - 1)})x_1$$

$$(x_4 - x_2)^2 + (y_4 - y_2)^2 = L^2\cos^2\psi$$

We know,

$$\theta = 180 - \alpha - \phi$$

where θ is the angle that bar 2 makes with the x-axis.

$$x_2 = L\cos\psi(\beta_2 - 1)\cos\theta$$

$$y_2 = x_2 \tan\theta$$

$$x_4 = x_2 + L\cos\psi\cos\theta$$

$$y_4 = (x_4 - x_2)tan\theta + y_2$$

$$x_5 = xi - a_x$$

$$y_5 = yi - a_y$$

where design parameters are $\beta_1, \beta_2, \psi, a_x$ and a_y whereas, α and ϕ are variables.

The new node matrix will be constructed on the basis of new x,y and z coordinates in the following sections where Protense design A and B are introduced.

3.3.3 Design Parameters selection

The position parameters in this formulation are β_1, β_2, a_x, a_y and ψ. The dimensional parameters are length of the planar bars, length of the non-coplanar bar and bars' outer and inner radii. The length of the planar bars is determined by the anthropometric measurements of a 50 percentile male and the dimension of the non-coplanar bar is chosen to facilitate the placement of the human knee width wise. The anthropometric data used to design the structure is given in table 3.1. The decision about the radii and material properties of the bars and strings is taken after conducting a static analysis of the structure, as discussed in section 5.2. The selection of a_x and a_y is made on the basis of positioning of the non-coplanar bar as per the height of amputation such that the bar always presses against lower portion of the above extremity. The variables are ϕ and α are approximated from human gait data to form functions in time.

3.3.4 String Elimination technique

Initially, the design had 5 bars and 32 strings for Design A and 42 strings for Design B. The degrees of freedom of the structure when no node is fixed is 25 (5 degrees of freedom per bar). This provides an opportunity in reduction in number of strings as well as optimization of actuator energy by removing the strings that are entirely redundant. One of the standard techniques for

selecting sensors and actuators is executed by using information architecture for bounded control energy and desired output co-variance. An ad-hoc method was developed in this work for the preliminary elimination of redundant strings which is described below:

The following steps were undertaken to obtain a feasible null space with all positive force densities:

- Step 1: Pick a null space with lowest number of negative or positive force densities. Aim is to obtain a null space with all the non zero values having same sign.
- Step 2: Eliminate the strings corresponding to the negative/ positive force densities.
- Step 3: Run the analysis again and obtain new null spaces.
- Step 4: Repeat Step 2 and Step 3 till you obtain a non trivial null space with all negative/ positive force densities.
- Step 5: Check if the resulting structure seems physically feasible and forces balance out.
- Step 6: If the structure does not seem stable, restore one or two strings back into the structure to make the structure feasible.
- Step 7: Check if you still obtain at least one non trivial null space with all negative/ positive force densities.
- Step 8: Keep repeating Step 6 and Step 7 till you obtain a desired configuration of bars and strings.

For example, static equilibrium was checked for with $\beta_1 = 0.1$ and $\beta_2 = 0.3$ with varying α $(80^o$ - $150^o)$ with 32 strings initially.

Nodes 1 and 7 are fixed to the ground and non-coplanar bar is not allowed to translate or rotate.

The matrix with external forces is given below:

$$W = \begin{Bmatrix} -60 & 60 & 0 & 0 & 0 & 0 & -60 & 60 & 0 & 0 \\ 0 & 0.6 & 0 & 0 & 0 & 0 & 0 & 0.6 & 0 & 0 \\ 0 & 0 & 0 & 0 & 0 & 0 & 0 & 0 & 0 & 0 \end{Bmatrix}$$

There were 13 null spaces bases found associated with free variables;

γ_{22}, γ_{24}, γ_{25}, γ_{26}, γ_{27}, γ_{30}, γ_{31}, γ_{32}, λ_1, λ_2, λ_3, λ_4 and λ_5 where strings 25 to 32 are the coupling strings.

Starting from 32 strings, the strings were eliminated as per the steps listed above. This resulted in the number of strings being reduced to just 14 strings. The total degrees of freedom of the system is 5x5=25 and number of constraints are 11, thus the available degrees of freedom are 14. The null space at this point was one. The existence of one null space indicates that there are infinite solutions for force densities that satisfy the static equilibrium condition for the structure and thus provides some scope for optimization.

The final connectivity matrix indices found are as follows:

$$C_{is} = \begin{Bmatrix} 2 & 3 & 4 & 1 & 3 & 4 & 8 & 9 & 6 & 6 \\ 4 & 1 & 5 & 5 & 5 & 9 & 10 & 7 & 9 & 10 \end{Bmatrix}$$

$$Cc_{is} = \begin{Bmatrix} 4 & 2 \\ 8 & 10 \end{Bmatrix}$$

The above matrices can be read as string 1 is connected from node 2 to node 4 and string 2 is connected from node 3 to node 1 and so on.

Above method was used to initially reduce the number of strings in ProTense for both designs A and B but owing to different boundary conditions and external forces in case of different phases, the above technique did not prove very useful. Additionally, some redundant strings are also needed for stability during dynamics which are added through trial and error.

The method that was finally used for preliminary string elimination is given below:

Step1: Run the static analysis for the entire range of motion for all combinations of α and ϕ.

Step2: Note the minimum norm solution given by MATLAB's function `linprog` for each of the configurations.

Step3: Eliminate the strings that are consistently accounting for zero force densities.

Step4: Check again for static equilibrium with eliminated strings.

The number of strings required for dynamic equilibrium are mostly more than that for the static due to addition of inertial forces, therefore additional strings are added post running the dynamic simulation.

3.3.5 Selection of structural properties for bars and strings

There are three materials considered for the bars; Aluminium, Brass and Carbon fibre whereas two materials are considered for the strings; Steel and Spectra. The properties of all materials are listed in Table 3.5. Same material and sizes are used for the bars and strings for both Design A and B.

Material	Young's Modulus	Density	Yield Strength
Steel	180 GPa	$8050kg/m^3$	250MPa
Aluminium	68.9 GPa	$2700kg/m^3$	240 MPa
Brass	110 GPa	$8400kg/m^3$	395MPa
Carbon fibre	228 GPa	$1600kg/m^3$	757MPa (compressive)
Spectra	117GPa	$970kg/m^3$	2.4GPa

Table 3.5: Material Properties.

First, radius of the bars and strings are determined using the static equilibrium by checking against the yielding and buckling conditions as given in equations 3.48. The resulting radii are then doubled and fed into the dynamic simulation to iteratively determine the minimal feasible mass for the structure as is described in the flow chart, 3.16.

$$F_b = \frac{E\pi^3 r_o^4}{4l} \tag{3.47}$$

$$\gamma_i s_i < \sigma_s \times A \tag{3.48}$$

Where, F_b is the maximum buckling force the bar can take before buckling, E is the Young's modulus, σ_s is the yield strength of the material for bar or string, r_o is the outer radius, l is the length and A is the area of the bar/string.

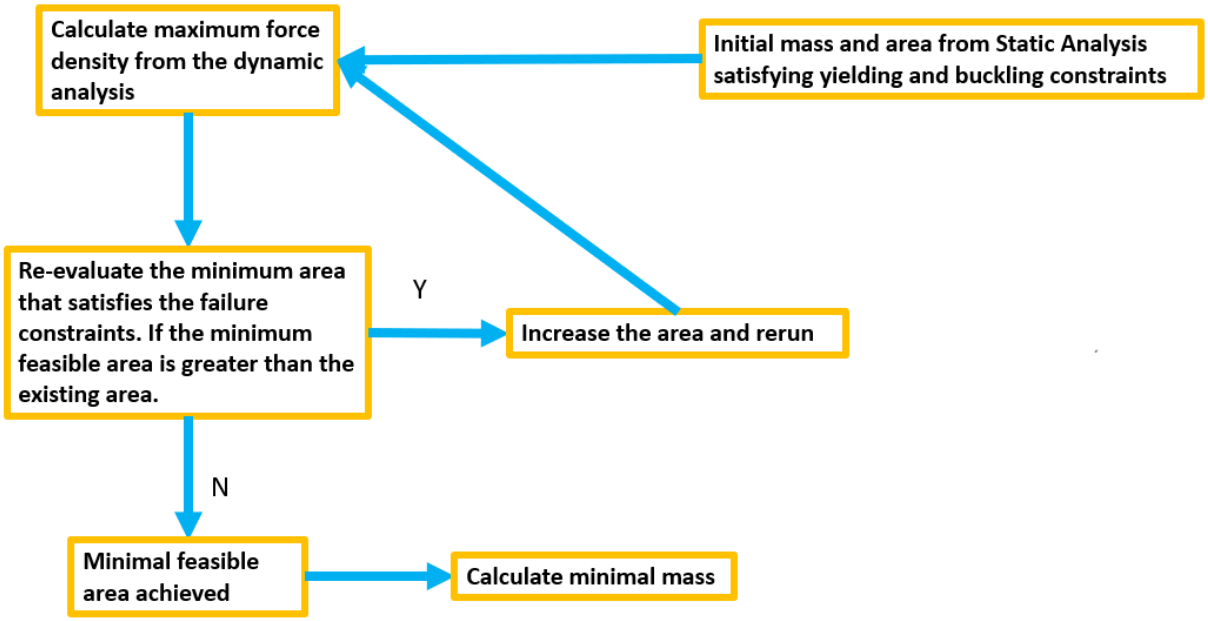

Figure 3.16: Mass Determination Flow Chart.

Minimum radius of the strings for no yielding is 0.88 mm. Final material selected for the simulation is Aluminium for bars and Spectra (ultra high molecular weight polyethylenefor strings. The selection of the radii of the bars and strings is decided after dynamic analysis and are mentioned separately for both, Design A and B in their respective sections.

3.3.6 Control of ProTense

The algorithm for the same is depicted in the flow chart in figure 3.17.

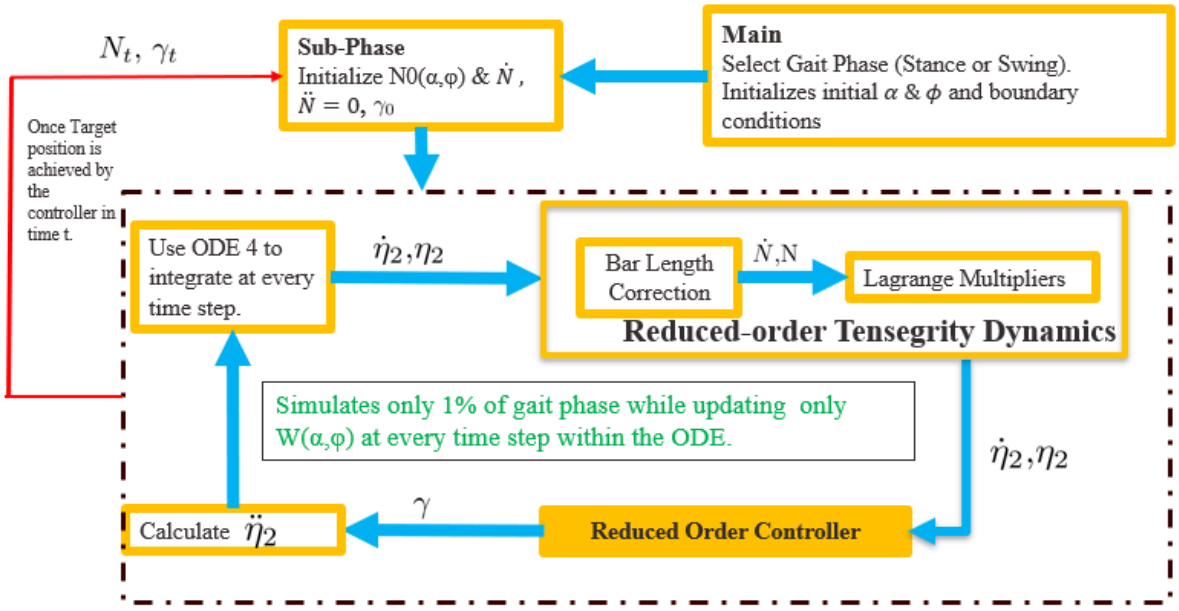

Figure 3.17: Algorithm to control Protense.

3.3.6.1 Pseudo Static Controller

Pseudo Static Controller was used as a preliminary control technique to check if a particular configuration can be achieved by rest length control for a series of different α and ϕ. Target rest lengths were obtained by interpolating the rest lengths obtained from conducting static equilibrium analysis on configurations posed by selected α and ϕ that span the entire range of motion of a leg. Rest length of each string act as the control variable to obtain different configurations. A plot showing the variation of 16 rest length values as α and ϕ varies in 50% stance and swing cycles are shown in figure 3.18 and figure 3.19 respectively.

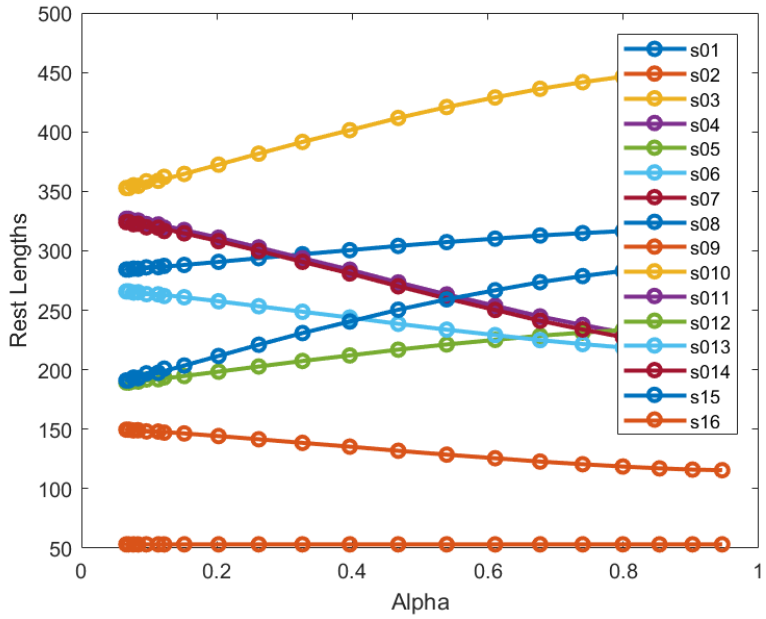

Figure 3.18: Rest length for swing plotted against alpha.

3.3.6.2 Second Order Error Dynamics Controller

Once the position of the target nodes to follow the gait trajectory are known, a second order differential equation is written in the error (E) between the current and target positions as

$$E = Y - \bar{Y} \tag{3.49}$$

$$E = LNR - \bar{Y}. \tag{3.50}$$

where L is an I_{na} matrix with na defining the number of axes (x,y,z) the nodes are desired to be controlled in, R ($n \times nt$) picks the nodes that are to be controlled and Y_t is a ($na \times nt$) matrix with n being the number of nodes and nt used for the number of target nodes.

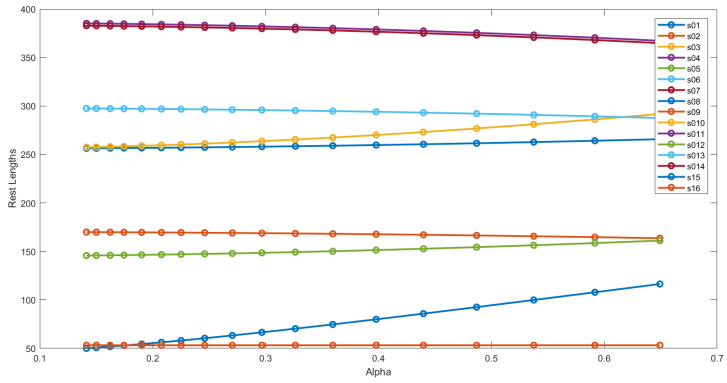

Figure 3.19: Rest length for stance plotted against alpha.

The second order differential equation to derive the error to zero can be written as

$$\ddot{E} + \Psi\dot{E} + \Theta E = 0 \tag{3.51a}$$

$$L\ddot{N}R + \Psi L\dot{N}R + \Theta(LNR - \bar{Y}) = 0 \tag{3.51b}$$

$$L(W + \Omega P^T - NK)M^{-1}R + \Psi L\dot{N}R + \Theta(LNR - \bar{Y}) = 0 \tag{3.51c}$$

where ψ and Θ are the control parameters to tune the frequency and damping of the second order system in E. From the previous derivation in section 5.2, we can substitute,

$$K = (C_s^T\hat{\gamma}C_s - C_b^T\hat{\lambda}C_b) \tag{3.52}$$

$$\hat{\lambda} = -\frac{1}{12}\hat{m}_b\hat{l}^{-2}\lfloor\dot{B}^T\dot{B}\rfloor - \frac{1}{2}\hat{l}^{-2}\lfloor B^T(W - S\hat{\gamma}C_s)C_b^T\rfloor$$

If we take the i^{th} diagonal of λ, we get

$$\lambda_i = -m_{bi}l_i^{-2}||\dot{b}_i||^2 - \frac{1}{2}l_i^{-2}b_i^T(W + \Omega P^T)C_b^T e_i + \frac{1}{2}l_i^{-2}b_i^T S(\widehat{C_s^T C_b^T e_i})\gamma \tag{3.53}$$

The equation 3.53 can be written as a linear function of γ, thus we can write

$$\lambda = \Lambda\gamma + \tau \tag{3.54}$$

where, i^{th} row of Λ can be written as

$$\begin{aligned}
\Lambda i^{th} row &= \frac{1}{2} l_i^{-2} b_i^T S(\widehat{C_s^T C_b^T e_i}) \\
\tau_i &= -m_{bi} l_i^{-2} ||\dot{b_i}||^2 - \frac{1}{2} l_i^{-2} b_i^T (W + \Omega P^T) C_b^T e_i \\
i &= 1, 2 \ldots\ldots \beta
\end{aligned}$$

On substituting $\hat{\lambda}$ in equation 3.52, we can re-write equation 3.51c in the form

$$\begin{bmatrix} \Gamma_1 \\ \Gamma_2 \\ \vdots \\ \Gamma_{n_r} \end{bmatrix} \gamma = \begin{bmatrix} \mu_1 \\ \mu_2 \\ \vdots \\ \mu_{n_r} \end{bmatrix}, \tag{3.55}$$

where,

$$\Gamma_i = LNC_s^T(C_s\widehat{M^{-1}}Re_i) - LNC_b^T(C_b\widehat{M^{-1}}Re_i)\Lambda \tag{3.56}$$

$$\mu_i = \Big(L(W + \Omega P^T)M^{-1}R + \Psi L\dot{N}R + \Theta(LNR - \bar{Y})\Big)e_i + LNC_b^T(C_b\widehat{M^{-1}}Re_i)\tau \tag{3.57}$$

Equation 3.55 can be posed as a linear algebra problem which can be solved to find the least square solution in MATLAB using the `lsqlin` function,

$$\begin{aligned}
\underset{\gamma}{Min} \quad & ||\Gamma\gamma - \mu||_2 \\
& s.t.\ \gamma \geq 0
\end{aligned} \tag{3.58}$$

The above controller is full order where all nodes positions, velocities and accelerations are fed

into the controller without providing the knowledge about the nodes that are constrained. Above controller dynamics can be written in reduced order form to provide a better controller that uses more accurate information regarding the system constraints.

3.3.6.3 Reduced Order Second Order Error Dynamics controller

The nodal coordinate matrix N can be transformed into a reduced order subspace using the transformation N=[$\eta_1 U_1$ $\eta_2 U_2$], where η_2 is associated with the nodes that are fixed and η_1 is associated with the free nodes and U=$[U_1, U_2]$ is a unitary matrix obtained from singular value decomposition (SVD) of P. The resulting error equation can be updated as:

$$E = L[\eta_1 \;\; \eta_2]U^T R - \bar{Y}. \tag{3.59}$$

Following the formulation of equation 3.51c, the second order differential equation can be re-written in terms of new coordinates η_1 and η_2 from equation 3.59.

$$\ddot{E} + \Psi\dot{E} + \Theta E = 0 \tag{3.60}$$

$$L\ddot{\eta_2}U_2^T R + \alpha L\dot{\eta_2}U_2^T R + \Theta[L(\eta_1 U_1^T + \eta_2 U_2^T)R - \bar{Y}] = 0 \tag{3.61}$$

$$L(WU_2 - \eta_1 U_1^T K U_2 - \eta_2 U_2^T K U_2)M_2^{-1}U_2^T R + \alpha L\dot{\eta_2}U_2^T R + \Theta[L(\eta_1 U_1^T + \eta_2 U_2^T)R - \bar{Y}] = 0 \tag{3.62}$$

On rearranging the above equation, we get,

$$L(\eta_1 U_1^T K U_2 + \eta_2 U_2^T K U_2)M_2^{-1}U_2^T R = \mathcal{C} \tag{3.63}$$

$$\mathcal{C} \triangleq LWU_2 M_2^{-1}U_2^T R + \alpha L\dot{\eta_2}U_2^T R + \Theta[L(\eta_1 U_1^T + \eta_2 U_2^T)R - \bar{Y}] \tag{3.64}$$

Further, on substituting $K = (C_s^T \hat{\gamma} C_s - C_b^T \hat{\lambda} C_b)$, we realize that the equation is linear in γ and

can be posed as linear program problem as

$$\begin{bmatrix} \Gamma_1 \\ \Gamma_2 \\ \vdots \\ \Gamma_{n_r} \end{bmatrix} \gamma = \begin{bmatrix} \mu_1 \\ \mu_2 \\ \vdots \\ \mu_{n_r} \end{bmatrix}, \tag{3.65}$$

where,

$$\begin{aligned} \Gamma_i &= LNC_s^T(\widehat{C_sMRe_i}) - LNC_b^T(\widehat{C_bMRe_i})\Lambda \\ \mu_i &= \mathcal{C}e_i + LNC_b^T(\widehat{C_bMRe_i})\tau \\ \mathcal{C} &= LWU_2M_2^{-1}U_2^TR + \alpha L\dot{\eta}_2U_2^TR + \Theta[L(\eta_1U_1^T + \eta_2U_2^T)R - \bar{Y}] \\ M &= U_2M^{-1}U_2^T \\ i &= 1, 2 \ldots n_r \end{aligned}$$

3.4 ProTense Design A

ProTense Design A is built for individuals with a disabled lower leg and a healthy upper leg. This design essentially works to transfer the momentum from the residual leg to move the prosthetic such that it follows the gait of a healthy person. Stance phase constitutes almost 60 % of the gait cycle for walking of an healthy individual. Assuming 1 % of gait is achieved in 0.1 seconds, the time needed to complete the stance phase is 6 seconds.

3.4.1 Layout

The structure of ProTense consists of 5 bars and 32 strings with 2 bars representing the upper leg and two bars for the lower leg. The fifth bar is used to cradle the leg and acts as the virtual knee.

Node matrix for design A can be written as:

$$N^A_{lst} = \begin{Bmatrix} \frac{x_i-(1-\beta_1)x_3}{\beta_1} & L\cos\psi(\beta_2-1)\cos\theta & x_i - L\beta_1\cos\phi & x_2 + L\cos\psi\cos\theta \\ \frac{y_i-(1-\beta_1)y_3}{\beta_1} & x_2\tan\theta & y_i + \beta_1(x_3-x_1)\tan\phi & y_2 + (x_4-x_2)\tan\theta \\ -0.4L_s & z_4 + L\sin\psi & -0.4L_s & -0.35L_s \end{Bmatrix}$$

$$N^A_{ust} = \begin{Bmatrix} x_1 & \frac{x_i-(1-\beta_2)x_4}{\beta_2} & x_1 - L\cos\phi & x_2 + L\cos\psi\cos\theta \\ y_1 & \frac{y_i-(1-\beta_2)y_4}{\beta_2} & y_1 + (x_3-x_1)\tan\phi & y_2 + (x_4-x_2)\tan\theta \\ 0.4L_s & -z_4 - L\sin\psi & 0.4L_s & -0.35L_s \end{Bmatrix}$$

$$N^A_{lsw} = \begin{Bmatrix} x_1 & \frac{x_i-(1-\beta_2)x_4}{\beta_2} & x_1 - L\cos\phi & x_2 + L\cos\psi\cos\theta \\ y_1 & \frac{y_i-(1-\beta_2)y_4}{\beta_2} & y_1 + (x_3-x_1)\tan\phi & y_2 + (x_4-x_2)\tan\theta \\ -0.4L_s & z_4 + L\sin\psi & -0.4L_s & -0.35L_s \end{Bmatrix}$$

$$N^A_{usw} = \begin{Bmatrix} x_1 & \frac{x_i-(1-\beta_2)x_4}{\beta_1} & x_1 - L\cos\phi & x_2 + L\cos\psi\cos\theta \\ y_1 & \frac{y_i-(1-\beta_2)y_4}{\beta_2} & y_1 + (x_3-x_1)\tan\phi & y_2 + (x_4-x_2)\tan\theta \\ 0.4L_s & -z_4 - L\sin\psi & 0.4L_s & -0.35L_s \end{Bmatrix}$$

$[N^A_{ust}, N^A_{ust}]$ and $[N^A_{lsw}, N^A_{usw}]$ are the matrices defining the lower and upper scissor node matrices for stance and swing respectively. The derivation of the above nodal matrices is given in section 3.3.4. x_i and y_i are the point of intersection of the two bars which are parametrized using a_x and a_y. The values of a_x and a_y change at different points of the gait phases. For swing, $a_x = 10$ and $a_y = 50$ throughout the phase while for stance,

$$[a_x, a_y] = \begin{cases} [10, 50], & \text{for first 60\% of stance} \\ [5, 50] & \text{for next 10\% of stance} \\ [10, 60] & \text{for next 5\% of stance} \\ [10, 50] & \text{for last 25\% of stance} \end{cases} \tag{3.66}$$

x_1 and y_1 in swing are taken as the hip coordinates at the end of transition phase which is same

as that at the end of stance as the hip node is fixed as we enter from stance into transition phase.

3.4.2 String configuration

Total number of strings in the structure are 25 with different strings getting active in different phases of the gait while the other strings remain passive (slack). The terminology of active and passive strings is explained in the section 3.2 and the final string configuration is shown in 3.20. The connectivity matrix for design A for bars and strings are given by C_b^A and C_s^A as:

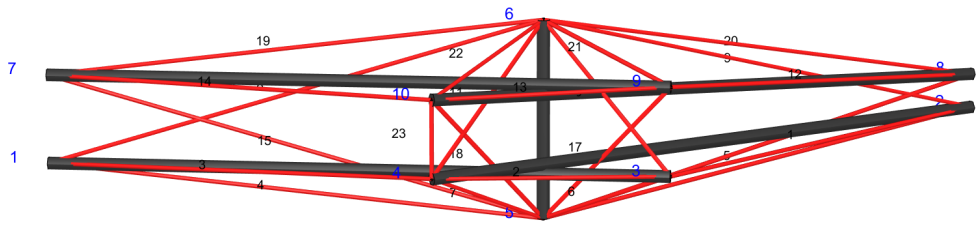

Figure 3.20: Design A with final string configuration. Black numbers show string number and blue digits indicate respective node numbers.

$$C_b^A = \begin{Bmatrix} 1 & 2 & 5 & 7 & 8 \\ 3 & 4 & 6 & 9 & 10 \end{Bmatrix} \tag{3.67}$$

$$C_s^A = \begin{Bmatrix} 2 & 3 & 4 & 1 & 2 & 3 & 4 & 1 & 2 & 3 & 4 & 8 & 9 & 10 & 5 & 5 & 5 & 5 & 6 & 6 & 6 & 6 & 4 \\ 3 & 4 & 1 & 5 & 5 & 5 & 5 & 6 & 6 & 6 & 6 & 9 & 10 & 7 & 7 & 8 & 9 & 10 & 7 & 8 & 9 & 10 & 10 \end{Bmatrix} \tag{3.68}$$

3.4.2.1 Stance

There are in total 17 strings that experience non-zero force density during the entire phase while there are some strings that get active only for a small portion of the gait. The remaining 8 strings always remain slack. The resulting string configuration can be defined as:

$$C_{sst} = \begin{Bmatrix} 3 & 4 & 1 & 4 & 1 & 2 & 3 & 4 & 9 & 10 & 5 & 5 & 5 & 6 & 6 & 6 & 4 \\ 4 & 1 & 5 & 5 & 6 & 6 & 6 & 6 & 10 & 7 & 8 & 9 & 10 & 7 & 9 & 10 & 10 \end{Bmatrix} \tag{3.69}$$

The strings experiencing maximum force density are S6, S9, S15 and S14.

3.4.2.2 Transition phase

Transition phase as expected, uses the minimum number of strings since only static equilibrium for this phase is modeled. All the strings get active in at different time steps of the transition phase.

$$C_{st} = \begin{Bmatrix} 2 & 3 & 4 & 1 & 2 & 3 & 4 & 2 & 8 & 9 & 10 & 5 & 6 & 6 & 6 & 4 \\ 3 & 4 & 1 & 5 & 5 & 5 & 5 & 6 & 9 & 10 & 7 & 8 & 7 & 8 & 9 & 10 \end{Bmatrix} \tag{3.70}$$

3.4.2.3 Swing

There are 18 strings that get active during the swing phase at some or the other time instant in the swing cycle. The most important strings are S10, S13, S16 and S19 which can be read from the string configuration matrix given below:

$$C_{ssw} = \begin{Bmatrix} 2 & 3 & 4 & 1 & 2 & 3 & 1 & 2 & 4 & 8 & 9 & 10 & 5 & 5 & 5 & 5 & 6 & 6 & 4 \\ 3 & 4 & 1 & 5 & 5 & 5 & 6 & 6 & 6 & 9 & 10 & 7 & 7 & 8 & 9 & 10 & 8 & 10 & 10 \end{Bmatrix} \tag{3.71}$$

3.4.3 Boundary conditions and External Forces

Design A assumes that Bar 1 and Bar 3 are strapped on individual's residual leg. One node of each of the bars is connected to the hip and the free node provides a point of attachment for the strings to control the prosthetic. This provides a channel for transferring momentum from the residual leg to the prosthetic.

3.4.3.1 Stance

Stance phase observes the foot being planted firmly on the ground while the upper extremity reorients to complete a step. Therefore, the nodes that are fixed for the stance phase are $[N_1, N_2, N_3, N_7, N_8, N_9]$, leaving only four free nodes. The primary external forces that act during the stance are the weight of the person and the ground reaction force and can be written with respect to the nodes index as

$$\begin{Bmatrix} -W_t & VGRf & 0 & 0 & 0 & 0 & -W_t & VGRf & 0 & 0 \\ 0 & -LGRf & 0 & 0 & 0 & 0 & 0 & LGRf & 0 & 0 \end{Bmatrix}$$

where, Wt denotes the weight of the individual, $VGRf$ is the vertical ground reaction force and $LGRf$ is the lateral ground reaction force.

3.4.3.2 Transition phase

Transition phase is modeled with one of the bar nodes of bar 1 and bar 3 fixed to the hip and the other node is kept free to move. Therefore, bars 1 and 3 have 2 degrees of freedom. The corresponding constraint matrix and the external force matrix can be written as

$$[N_1, N_7]$$

$$\begin{Bmatrix} -W_t & VGRf & 0 & 0 & 0 & 0 & -W_t & VGRf & 0 & 0 \\ 0 & -LGRf & 0 & 0 & 0 & 0 & 0 & LGRf & 0 & 0 \end{Bmatrix}$$

3.4.3.3 Swing

Swing phase comprises of the no-ground-contact portion of the gait phase where design A assumes that bar 1 and bar 3 are affixed to the thigh such that they move as the individual moves his upper leg and the strings attached to this bars pull the prosthetic's lower bars to complete the phase. External forces considered in this phase are the reaction forces on the hip node and the mass of the leg/ prosthetic depending on whether the individual is amputated or not. The resulting constraint matrix and external forces matrix can be formulated as

$$[N_1, N_3, N_7, N_9]$$

$$\begin{Bmatrix} Rf_1 & -\frac{m_L g}{2} & 0 & -\frac{m_L g}{2} & 0 & 0 & Rf_1 & -\frac{m_L g}{2} & 0 & -\frac{m_L g}{2} \\ Rf_2 & 0 & 0 & 0 & 0 & 0 & Rf_2 & 0 & 0 & 0 \end{Bmatrix}$$

where Rf_1 and Rf_2 are the reaction forces on the hip in the x and y directions and are evaluated in section 3.2, using a damped double pendulum and m_L is the mass of the leg or prosthetic.

3.4.4 Static Equilibrium Analysis

Using the above matrices for nodes, connectivity matrices, external forces and constraints, the structure is checked for static equilibrium for the entire range of ϕ and α angles to produce one complete step of the gait profile. Using the equation $NK = W$, we can convert it into a linear algebra problem, $Ax = b$. Matrix A is column rank deficient which indicates infinitely many non-zero values of x that can satisfy the equilibrium equation. Using the simplex algorithm of linprog, the problem is posed in MATLAB as

$$\begin{aligned} &\text{Minimize } C^T x \\ &\text{subject to :} \\ &Ax = b, \\ &x \geq 0, \end{aligned} \tag{3.72}$$

where C is a column matrix of dimension $(n_s + n_b)$ consisting of all ones with n_b and n_s denoting the number of bars and strings in the structure respectively. x is a column matrix comprising of all the force densities (λ and γ). Since we desire to have all the strings in tension and bars in compression, the non-negativity constraint is put on the force densities. b is a column matrix of external forces and A is defined as the componentized $NC_s^T C_{s_i} - NC_b^T C_{b_i}$, as explained in section 5.2. The resulting optimal equilibrium γs are noted for the entire gait cycle which can be fed into the dynamic simulation. The profile for the equilibrium γs is calculated separately for each phase according to their different boundary conditions and external forces as are depicted in figure 3.21a and figure 3.21b. The black lines are the bars and dotted red are the strings. The green lines in the figure indicates the direction of the external forces, and the black dot indicates the nodes that are fixed.

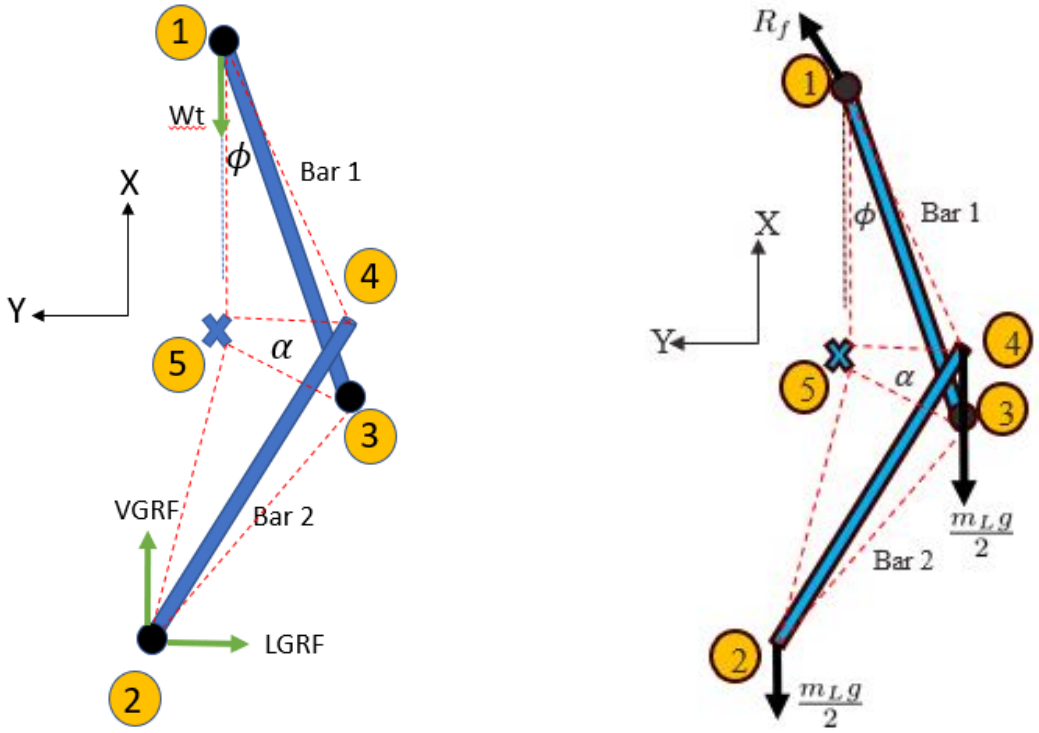

(a) Stance phase.

(b) Swing phase.

Figure 3.21: Phase wise design A boundary conditions, external forces and strings configuration in x-y plane. All the strings are not shown.

3.4.4.1 Stance

Owing to the boundary conditions, there is no net external force on the structure due to which the minimum force densities required in all the strings for static equilibrium is zero.

3.4.4.2 Transition phase

Transition phase is modeled by obtaining static equilibrium at every point and the optimal force densities (γ) are recorded to be used as controller inputs. The profile of equilibrium γ for transition phase is shown in figure 3.22b.

Transition phase from stance to swing is modeled from the 58% to 61% part of the gait cycle which includes terminal stance, double support and pre-swing phases. The external forces that act on the foot as lateral and vertical ground reaction force are applied on Nodes 2 Node 8. Equal and opposite force is applied on the Hip node (Nodes 1&7). The torque, acting on the structure due to the external forces described above, is balanced by a torque (equivalent to Hip Torque applied in real) expressed by two forces acting on the hip bar (Bar 1 and Bar 4) as shown in the figure 3.22a. The green lines in the figure indicates the direction of the external forces and the black dot indicates the nodes that are fixed.

3.4.4.3 Swing

There are 18 active strings used in swing with corresponding equilibrium force densities varying as displayed in the figure 3.23.

3.4.5 Controlled Dynamics

Dynamic simulation is run only for stance and swing. A second order controller is designed by writing a second order differential equation in the variable E, which denotes the error in the positions of the nodes from desired targets. The underlying theory and derivation of the error second order equation (3.73) in terms of node coordinates (N^A), force densities (γ^A, λ^A), constraint (Ω^A) and external forces (W^A) is derived in the section 3.4.3.

$$\ddot{E^A} + \psi \dot{E^A} + \Theta E^A = 0 \tag{3.73}$$

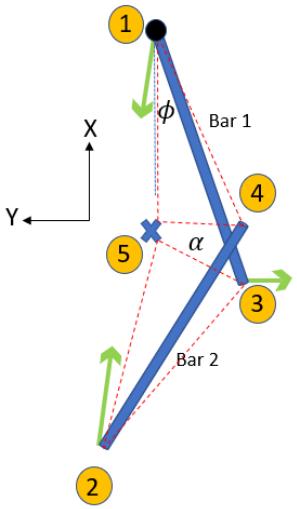

(a) Transition phase for Design A with boundary conditions, external forces and strings configuration in x-y plane.

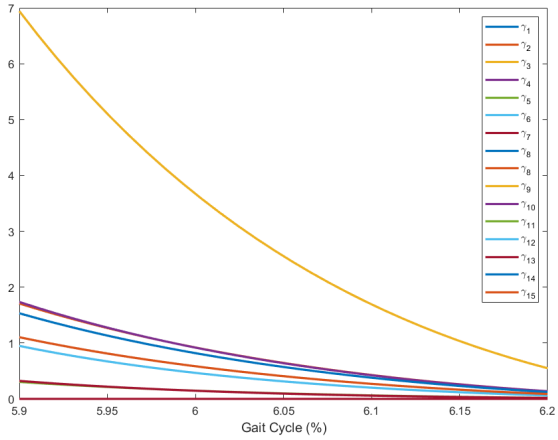

(b) Equilibrium force density in strings (γ) for swing phase in design A post static analysis.

Figure 3.22: Static analysis of transition phase for design A.

where $E^A = Y^A - Y_t^A$, the expressions for which differ for both the phases and are described in separate paragraphs below. The control parameters ψ and Θ play a crucial role in defining the characteristics of the error profile in terms of damping, rise time, overshoot etc. Different parameters are chosen for stance and swing to get an overdamped system for both the phases.

3.4.5.1 Stance

As can be recalled from sub-section 3.3.6,

$$Y_{st}^A = LN_{st}^A R_{st}^A \tag{3.74}$$

$$R_{st}^A = \begin{Bmatrix} 1 & 2 & 3 & 7 & 8 & 9 \end{Bmatrix}$$

Control parameters $\psi = 18$ and $\Theta = 30$ were selected for a resulting dynamical system with damping coefficient ($\eta = 1.04$). The error profile for all the nodes for stance is shown in figure 3.24. The evolution of γ calculated by the controller using linear least square algorithm are shown

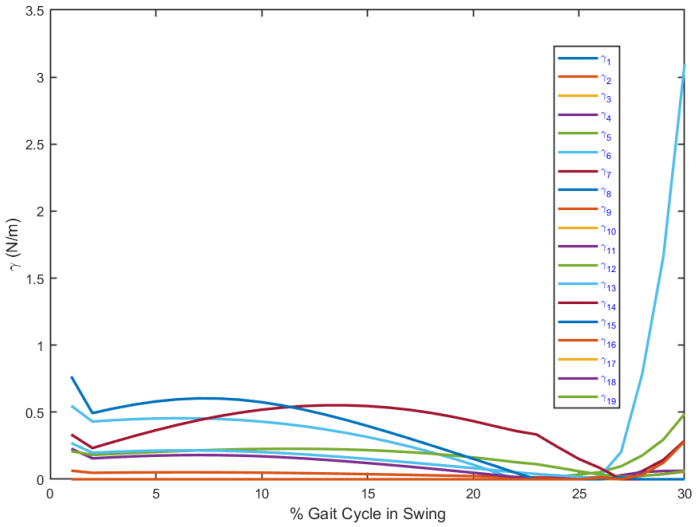

Figure 3.23: Equilibrium force density in strings (γ) for swing phase in design A post static analysis.

in figure 3.27.

3.4.5.2 Swing

Similarly, for swing phase

$$Y_{sw}^{A} = LN_{sw}^{A} R_{sw}^{A}$$

where,

$$R_{st}^{A} = \begin{Bmatrix} 1 & 3 & 7 & 9 \end{Bmatrix}$$

$\psi = 18$ and $\Theta = 30$ leading to a damping coefficient ($\eta = 1.04$) was used for swing. The error profile for the all the nodes for swing is shown in figure 3.26.

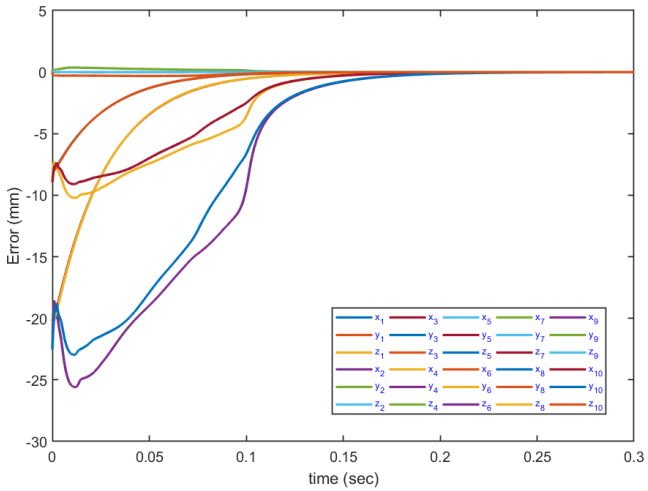

Figure 3.24: Evolution of errors in nodal coordinates for some gait % in stance for design A.

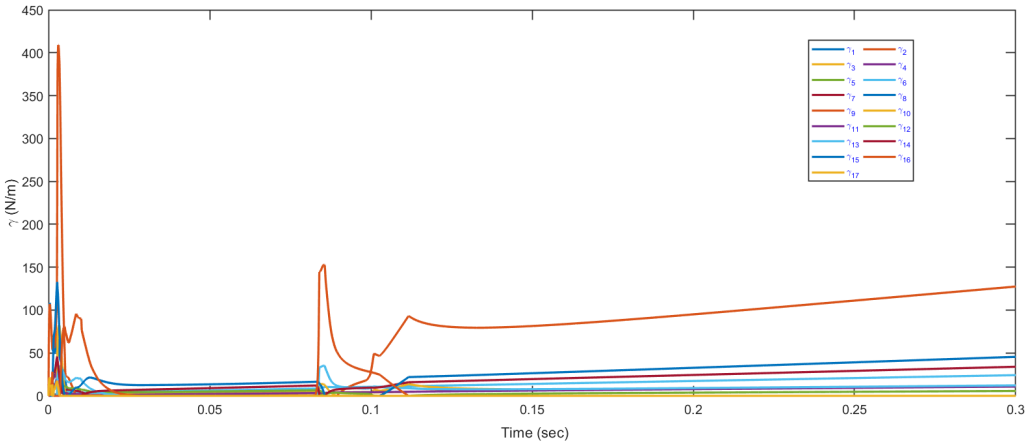

Figure 3.25: Evolution of γ for some discrete points of the gait cycle in the stance phase.

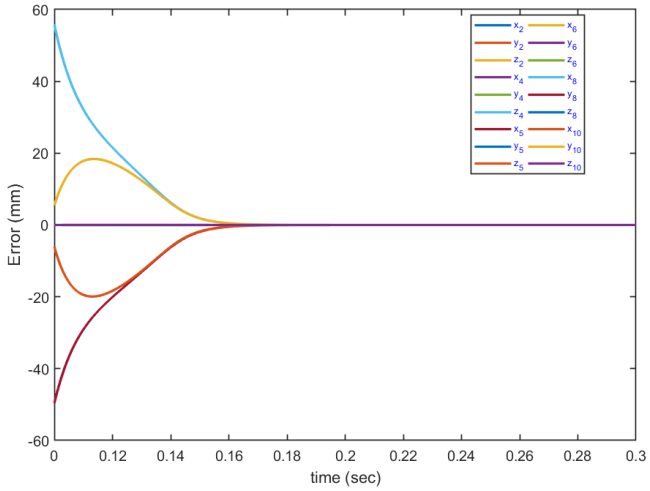

Figure 3.26: Evolution of errors in nodal coordinates for some gait % in swing for design A.

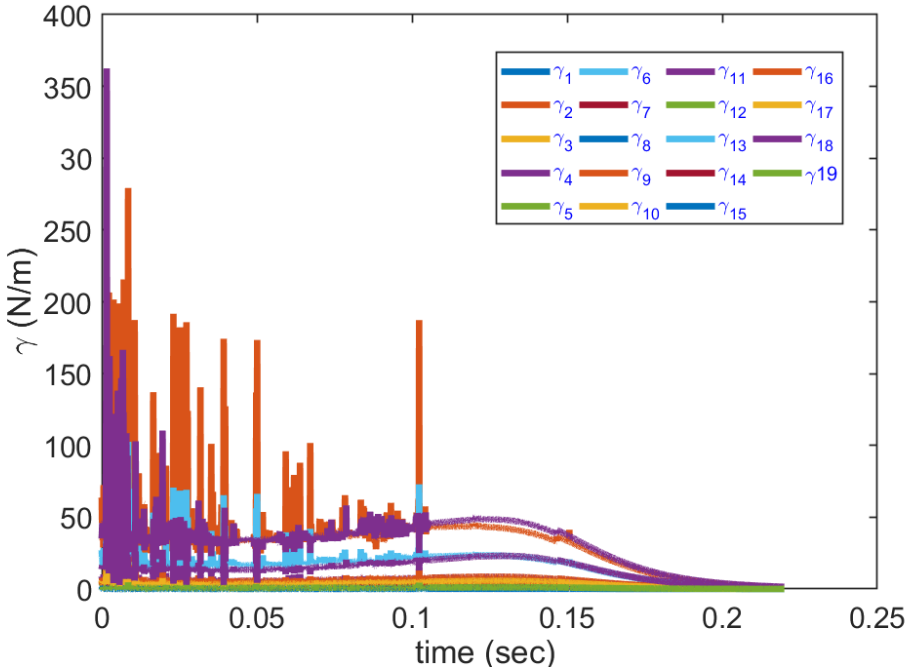

Figure 3.27: Evolution of γ for some discrete points of the gait cycle in the swing phase for Design A.

where L is a 3x3 identity matrix.

3.5 ProTense Design B

ProTense Design A is built to cater to the needs of an above/below knee amputee with a weak residual leg. This design has additional strings which are fixed at one end to the lower part of the torso to work like the hip muscles of a healthy individual. Four additional string nodes are added to the design. These nodes are fixed on the lower torso of the individual and were inspired by how hip muscles contract to provide the requisite torque for walking. A representative picture of activation of flexure and extensor muscles in a cat is shown in figure 3.28 The resulting node matrix looks like:

$$N^B_{lst} = \begin{pmatrix} \frac{x_i-(1-\beta_1)x_3}{\beta_1} & L\cos\psi(\beta_2-1)\cos\theta & x_i-L\beta_1\cos\phi & x_2+L\cos\psi\cos\theta & x_1-10 & x_1+10 \\ \frac{y_i-(1-\beta_1)y_3}{\beta_1} & x_2\tan\theta & y_i+\beta_1(x_3-x_1)\tan\phi & y_2+(x_4-x_2)\tan\theta & y_1-50 & y_1+50 \\ -0.4L_s & z_4+L\sin\psi & -0.4L_s & -0.35L_s & -0.4L_s & -0.4L_s \end{pmatrix}$$

$$N^B_{ust} = \begin{pmatrix} x_1 & \frac{x_i-(1-\beta_2)x_4}{\beta_2} & x_1-L\cos\phi & x_2+L\cos\psi\cos\theta & x_1-10 & x_1+10 \\ y_1 & \frac{y_i-(1-\beta_2)y_4}{\beta_2} & y_1+(x_3-x_1)\tan\phi & y_2+(x_4-x_2)\tan\theta & y_1-50 & y_1+50 \\ 0.4L_s & -z_4-L\sin\psi & 0.4L_s & -0.35L_s & 0.4L_s & 0.4L_s \end{pmatrix}$$

$$N^B_{lsw} = \begin{pmatrix} x_1 & \frac{x_i-(1-\beta_2)x_4}{\beta_2} & x_1-L\cos\phi & x_2+L\cos\psi\cos\theta & x_1-10 & x_1+10 \\ y_1 & \frac{y_i-(1-\beta_2)y_4}{\beta_2} & y_1+(x_3-x_1)\tan\phi & y_2+(x_4-x_2)\tan\theta & y_1-50 & y_1+50 \\ -0.4L_s & z_4+L\sin\psi & -0.4L_s & -0.35L_s & -0.4L_s & -0.4L_s \end{pmatrix}$$

$$N^B_{usw} = \begin{pmatrix} x_1 & \frac{x_i-(1-\beta_2)x_4}{\beta_1} & x_1-L\cos\phi & x_2+L\cos\psi\cos\theta & x_1-10 & x_1+10 \\ y_1 & \frac{y_i-(1-\beta_2)y_4}{\beta_2} & y_1+(x_3-x_1)\tan\phi & y_2+(x_4-x_2)\tan\theta & y_1-50 & y_1+50 \\ 0.4L_s & -z_4-L\sin\psi & 0.4L_s & -0.35L_s & 0.4L_s & 0.4L_s \end{pmatrix}$$

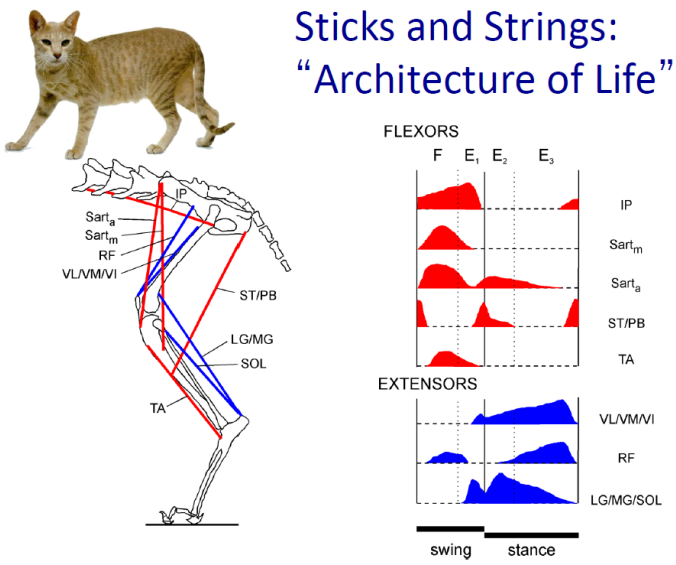

Figure 3.28: Muscular activation shown for a cat during normal walking.*

3.5.1 Strings configuration

Since the design B is modeled to control more degrees of freedom, it has more number of actuators (strings) in comparison with design A. The string configuration is shown via numbered strings and nodes in figure 3.29. The connectivity matrix showing string indexing for Design B can be written as:

$$C_{ss}^{B} = \begin{Bmatrix} 1 & 2 & 3 & 4 & 1 & 2 & 3 & 4 & 1 & 2 & 3 & 4 & 7 & 8 & 9 & 10 & 5 & 5 & 5 & 5 & 6 & 6 & 6 & 6 \\ 2 & 3 & 4 & 1 & 5 & 5 & 5 & 5 & 6 & 6 & 6 & 6 & 8 & 9 & 10 & 7 & 7 & 8 & 9 & 10 & 7 & 8 & 9 & 10 \end{Bmatrix}$$

$$C_{sh}^{B} = \begin{Bmatrix} 3 & 3 & 4 & 5 & 6 & 9 & 9 & 10 \\ 11 & 12 & 11 & 13 & 13 & 14 & 14 & \end{Bmatrix}$$

$$C_{c}^{B} = \begin{Bmatrix} 1 & 2 & 4 & 4 & 1 & 2 & 3 \\ 7 & 8 & 10 & 9 & 8 & 7 & 9 \end{Bmatrix}$$

$$C_{s}^{B} = \begin{Bmatrix} C_{ss}^{B} & C_{sh}^{B} & C_{c}^{B} \end{Bmatrix}$$

*Reprinted with permission from "Tensegrity Systems", by Robert E. Skelton, Mauricio C. de Oliveira, 2009, Springer Nature, Boston, MA. Coyright [2009] Springer-Verlag US.

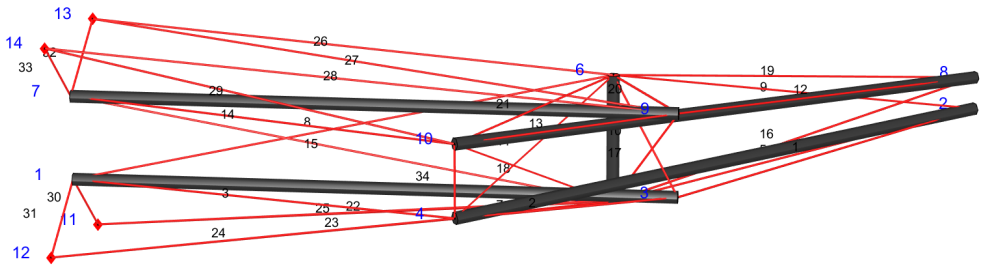

Figure 3.29: Design B with final string configuration. Black numbers show string number and blue digits indicate respective node numbers.

where, C_{ss}^{B} are the strings that denote bar to bar connections, C_{sh}^{B} denotes the strings connecting the hip nodes (string nodes) to bar nodes and C_{c}^{B} is used for the strings coupling strings between the two scissor structures. The configuration remains more or less the same for all the phases. It is observed that almost all 39 strings in design B participate at different times of each phase though some strings are in higher tension for actuation than others in the three phases which are detailed below.

3.5.1.1 Stance

During stance, the strings that are actuated the most are strings S3, S10, S18 and S20.

3.5.1.2 Swing

Since foot nodes (Node 2 and Node 8) are not fixed in swing as they are in stance, the strings that experience highest tension are the strings connecting the non-coplanar bar to the knee nodes (nodes 3,4,9 and 10) and the strings connecting the foot to the knee.

3.5.2 Boundary conditions and External Forces

External forces applied here are identical to the external forces applied in design A but the boundary conditions differ for design B as shown in table 3.6.

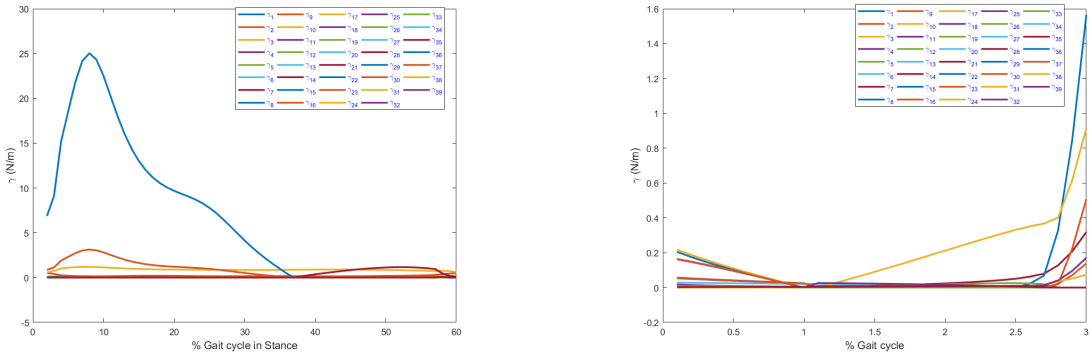

(a) Stance. (b) Swing.

Figure 3.30: Force densities resulting from static equilibrium analysis for design B.

Phase	Boundary Conditions
Stance	$[N_2, N_8, N_{11}, N_{12}, N_{13}, N_{14}]$
Swing	$[N_1, N_7, N_{11}, N_{12}, N_{13}, N_{14}]$
Transition	$[N_1, N_7, N_{11}, N_{12}, N_{13}, N_{14}]$

Table 3.6: Phase-wise boundary conditions displaying the fixed nodes in design B.

3.5.3 Static Equilibrium Analysis

As explained in section 3.4.4, static equilibrium was tested with the described external forces, boundary conditions and set of actuators for all three phases. Equilibrium γ plotted for the entire gait cycle are shown in figures 3.30a, 3.30b and 3.31.

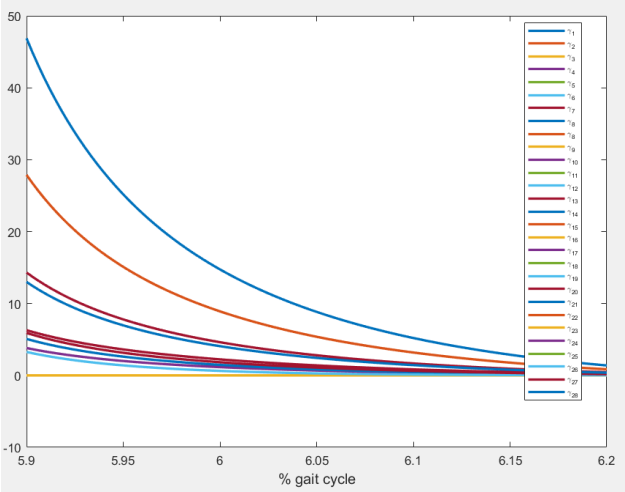

Figure 3.31: Static equilibrium force densities γ for transition phase.

3.5.4 Controlled Dynamics

Second order error dynamics controller was used to control the structure to obtain desired string force densities to produce a gait profile. The x,y and z coordinates of the nodes that were controlled in swing and stance are:

$$R_{st}^{B} = \begin{Bmatrix} 3 & 4 & 5 & 6 & 9 & 10 \end{Bmatrix}$$
$$R_{sw}^{B} = \begin{Bmatrix} 2 & 3 & 4 & 5 & 6 & 8 & 9 & 10 \end{Bmatrix}$$

With the $\psi = 1500$ and $\Theta = 10$, the system is overdamped with evolution of node errors ($\|E = Y_i - Y_{t_i}\|$) plotted in figure 3.32 for stance and 3.33 for swing as the controller brings the errors to zero and the evolution of all force densities is shown in figure 4.1a.

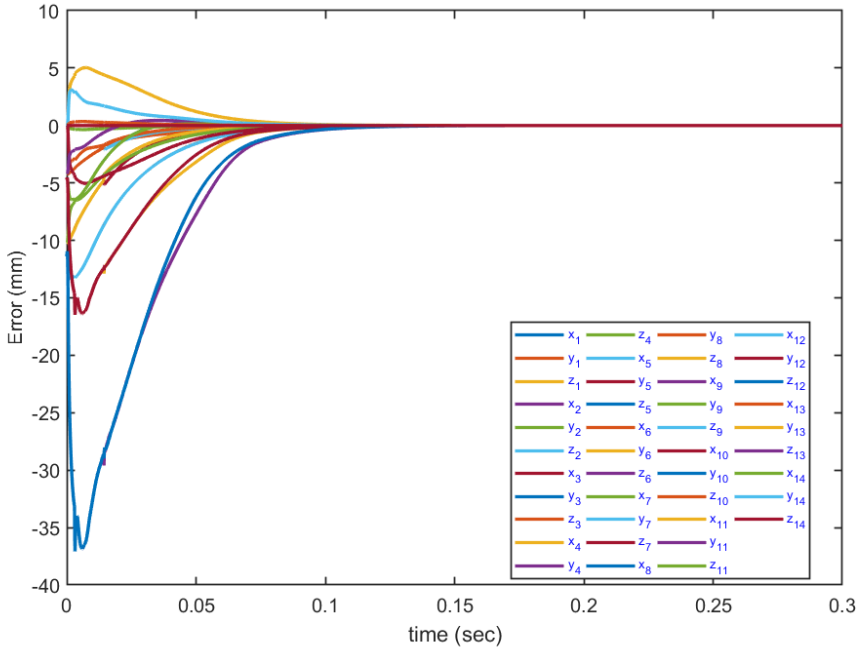

Figure 3.32: Evolution of errors in nodal coordinates for design B for some gait % case in stance.

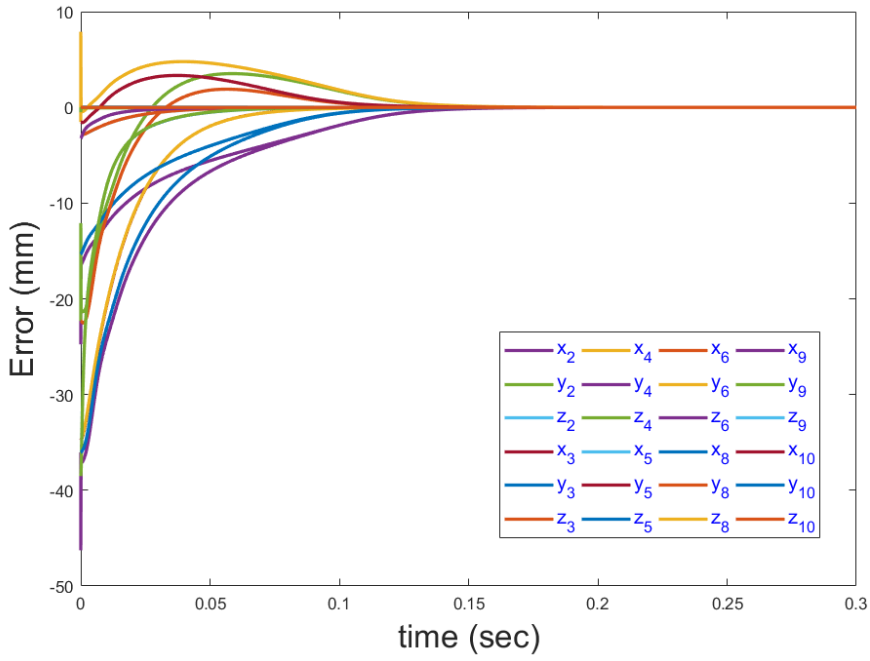

Figure 3.33: Evolution of errors in nodal coordinates for design B for some gait % case in swing.

Tensegrity Prosthetic leg was built for above/below knee amputees for individuals with working hip muscles (Design A) and weak hip muscles (Design B). Second order controller was used to control the movement of the two designs to match the gait of an individual on flat ground.

4.1 Numerical Simulation

A customized integrator that uses fixed time steps was used to integrate the velocity and acceleration of the nodes of the bars. Bar length correction was done at each time step of the integrator to ensure constant bar length throughout the simulation. For faster decay of error especially for Protense design B, the step size chosen for the integrator was of the order (1e-5) to curb the growing numerical error.

4.1.1 Bar length correction

Due to growing numerical errors while integrating this highly non-linear problem, the bar length of the bars change numerically. Since, the bars are considered rigid in this formulation, the positions of the nodes have to be corrected additionally using the least square algorithm given by Skelton et al.

Therefore, to resolve the discrepancies in bar length constraints in equations, $b^T b \neq l^2, b^T \dot{b} \neq 0$, Skelton introduces '**p**' and '**r**' as correction vectors for the two equations respectively and evaluate '**p**' and '**r**' vectors using the theorem given below:

Theorem: For any given **b**, $\dot{\mathbf{b}}$

$$Minimize \;\; J(\mathbf{p}, \mathbf{r}) = q||\mathbf{p}||^2 + ||\mathbf{r}||^2 \tag{4.1}$$

$$subject\ to \;\; ||\mathbf{b} + \mathbf{p}|| = l, \tag{4.2}$$

$$(\mathbf{b} + \mathbf{p})^T(\dot{\mathbf{b}} + r) = 0 \tag{4.3}$$

$$\mathbf{p} = l\mathbf{v} - \mathbf{b} \tag{4.4}$$

$$\mathbf{r} = -\mathbf{v}\mathbf{v}^T\dot{\mathbf{b}} \tag{4.5}$$

$$\mathbf{v} = [c\mathbf{I} + \dot{\mathbf{b}}\dot{\mathbf{b}}^T]^{-1} q l \mathbf{b} \tag{4.6}$$

$$x^4 + a_3 x^3 + a_2 x^2 + a_1 x + a_0 = 0 \tag{4.7}$$

$$a_3 = 2||\dot{\mathbf{b}}||^2 \tag{4.8}$$

$$a_0 = (ql)^2 ||\dot{\mathbf{b}}||^2 ((\mathbf{b}^T\dot{\mathbf{b}})^2 - ||\mathbf{b}||^2 ||\dot{\mathbf{b}}||^2) \tag{4.9}$$

$$a_1 = 2(ql)^2 ((\mathbf{b}^T\dot{\mathbf{b}})^2 - ||\mathbf{b}||^2 ||\dot{\mathbf{b}}||^2) \tag{4.10}$$

$$a_2 = ||\dot{\mathbf{b}}||^4 - (ql)^2 ||\mathbf{b}||^2 \tag{4.11}$$

4.2 Results

The major objective of an efficient prosthetic is to add aesthetic, physical and psychological value to the patient's experience such that the artificial leg mimics the real leg as closely as possible.

The two designs proposed in this study are essentially built for individuals with different levels of disabilities. Since the control of Protense design B is more independent of the movements of the individual, the evolution of its string force densities at different % of gait cycle is more comparable to forces experienced when biological muscles are activated.

The final mass of the prosthetic design was found to be 1.15Kg. To quantify how well the gait trajectory is followed in Design A & B, the errors at accrued at every 1 % of gait progression is expressed in terms of mean and standard deviation values. Figures 4.2 and 4.3 depict the evolution of mean and standard deviation in error values for the entire gait for design A and B respectively. This helps in giving some understanding of the evolution of errors at every time step and provides some bounds the error profile adheres to, while producing 100% of target gait trajectory.

Entire gait is discretized by 1% gait advances and the tension in the strings is normalized by the maximum string tension at that discretized point. The strings are color coded in figure 4.9

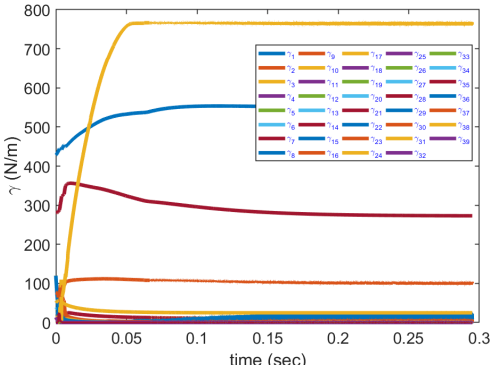

(a) Evolution of the force densities for stance phase.

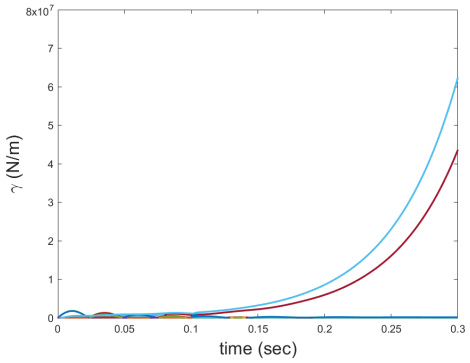

(b) Evolution of the force densities for swing phase.

Figure 4.1: Force density profiles during swing and stance for design B.

for swing and stance phase for both design A & B, to categorize the amount of tension in all the strings. Here, red indicates maximum extension, purple marks the second most tensed strings, yellow the third most tensed and green marks the least tensed strings, while grey lines indicate all the other strings. The strings that are maximally loaded in design B vary for different gait % but the strings connecting the non-coplanar bars with the scissor bars is always among the strings that experience maximum tension. The node connectivity pertaining to each string can be read from the string configuration index matrix given in equation 3.75.

The forces on the nodes of the non-coplanar bar are recorded to measure the amount of pressure and equivalent discomfort the bar causes to the residual leg and are depicted in figure 4.5a and 4.5b. This pressure in a comfortable range can be considered desired from a psychological point of view of the amputee. The identically zero force experienced at the nodes 5 & 6 post mid stance can be considered to be resulting from the vertical alignment of the foot with the torso during midstance. As the load profile shifts and the alignment of the body changes from pre-stance to post stance, the strings holding the non-coplanar bars are tensed in a way that the net force on the nodes 5 and 6 is zero indicating that the non-coplanar bar is softly resting against the back of the knee. The net ground reaction force on the foot is checked by measuring the net force on node 2 of the structure as shown in figure 4.4. This is comparable to the ground reaction force experienced by the foot during stance as shown in figures 3.9 and 3.10.

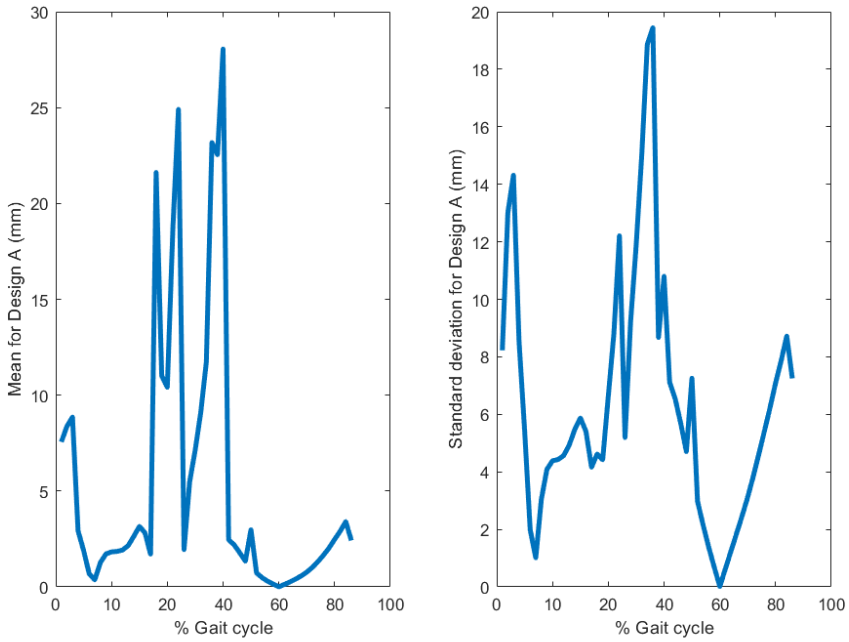

Figure 4.2: Mean and standard deviation of errors for design A for the entire gait.

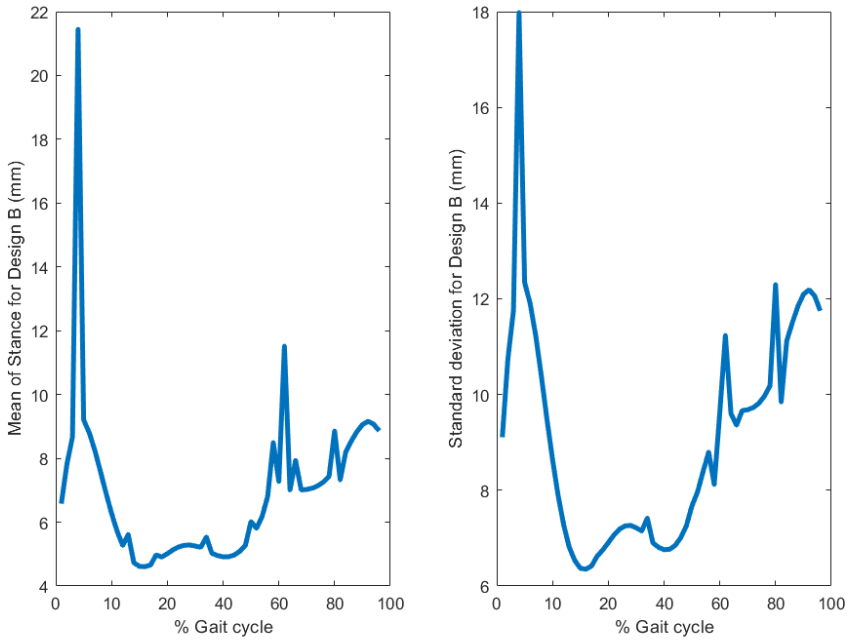

Figure 4.3: Mean and standard deviation of errors for design B for the entire gait.

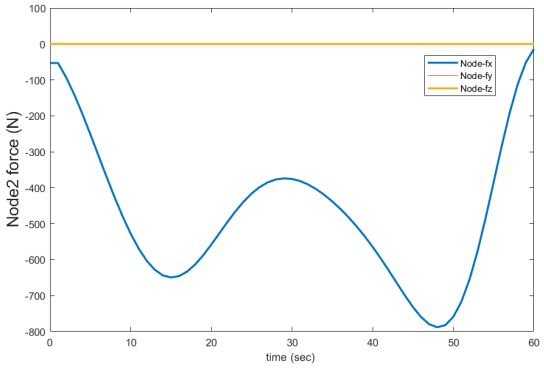

Figure 4.4: Profile of reaction force (N) experienced on Foot node (2 and 8) for design A

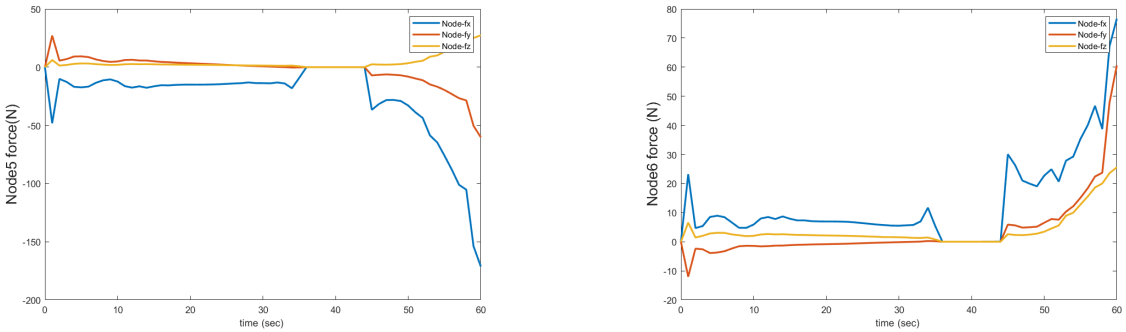

(a) Profile of reaction force (N) experienced on non-coplanar bar node 5.

(b) Profile of reaction force (N) experienced on non-coplanar bar node 6.

Figure 4.5: Force exerted by non-coplanar bar at the back of the knee/residual leg for design A.

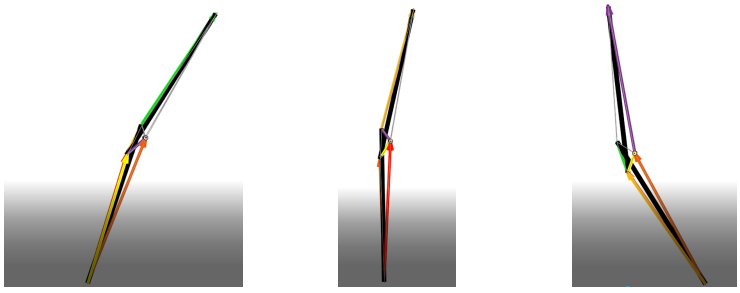

(a) 5% Gait cycle (stance) in Design A.

(b) 30% Gait cycle (stance) in Design A.

(c) 58% Gait cycle (stance) in Design A.

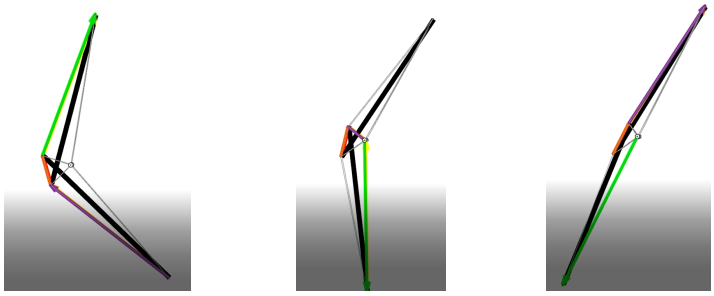

(a) 65% Gait cycle (swing) in Design A. (b) 80% Gait cycle (swing) in Design A. (c) 98% Gait cycle (swing) in Design A.

(a) 5% Gait cycle (stance) in Design B. (b) 30% Gait cycle (stance) in Design B. (c) 58% Gait cycle (stance) in Design B.

(a) 65% Gait cycle (swing) in Design B. (b) 80% Gait cycle (swing) in Design B. (c) 98% Gait cycle (swing) in Design B.

Figure 4.9: Highlighted strings for the entire gait for designs A & B.

5. SUMMARY, CONCLUSIONS AND FUTURE SCOPE

5.1 Summary and Conclusion

The current work focuses on the mathematical and computational aspects of a tensegrity leg with the potential to obtain human like gait in the sagittal plane. Two designs are proposed in the study with design A catering to the requirements of an amputee with a functional upper leg and Design B for individuals with a weak residual leg. We could match the gait of the prosthetic as per the data of a walking healthy individual for both design A and B. The data was discretized into % gait cycle with 1% increments to achieve one step. Design A requires input from the upper leg of the individual to control the lower leg prosthetic for following the gait trajectory while design B assumes complete control with strings acting like the muscles of individual's lower body.

The strings of the prosthetic design are actuated by a motor where each string is assumed to require an individual motor. The motors can be fitted on the lower part of the human torso, away from the point of actuation. This freedom in placement of motors reduces the the control energy requirement needed to lift the weight added by the motors as compared to when they are attached to the leg in the case of traditional prosthetic. The two thigh bars are considered to be strapped on the thighs of the individual but the physical fitting of the prosthetic on the leg and the placement of sensors and motors have not been evaluated.

This work is a computational demonstration of how a human leg can be replaced by an equivalent tensegrity prosthetic supporting the beliefs of Dr. Stephen Levid MD, who coined the term 'biotensegrity'. This work is in line with his idea of applying the concepts of tensegrity modelling to biological structures where the bones are like compression elements floating in the interstices of a complex tension network.

5.2 Future Scope

Design A and B can be considered as preliminary designs which have a huge scope of improvement. Firstly, in order to make this prosthetic operational for amputees, foot modelling is not

only necessary but also one of the most challenging task. Secondly, improved controller for faster gait (1 sec per step) is also of prime importance for a natural walking gait. Thirdly, placement of motors and determination of the total weight of the prosthetic along with the weight of motors and electronics is the next logical step.

Here, the simulation is done using cylindrical bars but for better fitting, the bars can be shaped (like bone-shaped) to increase the area of contact with the skin to reduce skin stresses at leg-prosthetic interface. In fact, smaller bars with K-class joints can be used to model the prosthetic for better adherence to the profile of the upper leg. Dynamics for tensegrity systems with massive strings has been developed by Skelton and should be used for a more realistic model of the prosthetic.

REFERENCES

[1] K. Ziegler-Graham, E. J. MacKenzie, P. L. Ephraim, T. G. Travison, and R. Brookmeyer, "Estimating the Prevalence of Limb Loss in the United States: 2005 to 2050," *Archives of Physical Medicine and Rehabilitation*, vol. 89, no. 3, pp. 422–429, 2008.

[2] T. R. Dillingham, L. E. Pezzin, and E. J. MacKenzie, "Limb amputation and limb deficiency: epidemiology and recent trends in the United States.," *Southern medical journal*, vol. 95, no. 8, pp. 875–83, 2002.

[3] M. F. Owings and L. J. Kozak, "Ambulatory and inpatient procedures in the United States, 1996.," *Vital and health statistics. Series 13, Data from the National Health Survey*, no. 139, pp. 1–119, 1998.

[4] M. Windrich, M. Grimmer, O. Christ, S. Rinderknecht, and P. Beckerle, "Active lower limb prosthetics: a systematic review of design issues and solutions," *From Robotics: Science and Systems*, vol. 28, 2013.

[5] A. Sabzi Sarvestani and A. Taheri Azam, "Amputation: a ten-year survey.," *Trauma monthly*, vol. 18, no. 3, pp. 126–9, 2013.

[6] P. Meade and J. Mirocha, "Civilian landmine injuries in Sri Lanka.," *The Journal of trauma*, vol. 48, no. 4, pp. 735–9, 2000.

[7] A. M. Dollar and H. Herr, "Lower Extremity Exoskeletons and Active Orthoses: Challenges and State-of-the-Art," *IEEE Transactions on Robotics*, vol. 24, no. 1, pp. 144–158, 2008.

[8] J. Feinglass, J. L. Brown, A. LoSasso, M. W. Sohn, L. M. Manheim, S. J. Shah, and W. H. Pearce, "Rates of lower-extremity amputation and arterial reconstruction in the United States, 1979 to 1996.," *American journal of public health*, vol. 89, no. 8, pp. 1222–7, 1999.

[9] H. Van Der Linde, J. Hofstad Cheriel, A. C. H. Geurts, K. Postema, J. H. B. Geertzen, and J. V. Limbeek, "A systematic literature review of the effect of different prosthetic components

on human functioning with a lower-limb prosthesis," Tech. Rep. 4, 2004.

[10] M. P. Murray, L. A. Mollinger, S. B. Sepic, G. M. Gardner, and M. T. Linder, "Gait patterns in above-knee amputee patients: hydraulic swing control vs constant-friction knee components.," *Archives of physical medicine and rehabilitation*, vol. 64, no. 8, pp. 339–45, 1983.

[11] S. J. Mattes, P. E. Martin, and T. D. Royer, "Walking symmetry and energy cost in persons with unilateral transtibial amputations: matching prosthetic and intact limb inertial properties.," *Archives of physical medicine and rehabilitation*, vol. 81, no. 5, pp. 561–8, 2000.

[12] S. A. Hale, "Analysis of the swing phase dynamics and muscular effort of the above-knee amputee for varying prosthetic shank loads.," *Prosthetics and orthotics international*, vol. 14, no. 3, pp. 125–35, 1990.

[13] A. M. Boonstra, J. Schrama, V. Fidler, and W. H. Eisma, "Energy cost during ambulation in transfemoral amputees: a knee joint with a mechanical swing phase control vs a knee joint with a pneumatic swing phase control.," *Scandinavian journal of rehabilitation medicine*, vol. 27, no. 2, pp. 77–81, 1995.

[14] A. Gitter, J. Czerniecki, and M. Meinders, "Effect of prosthetic mass on swing phase work during above-knee amputee ambulation.," *American journal of physical medicine & rehabilitation*, vol. 76, no. 2, pp. 114–21, 1997.

[15] E. Isakov, Z. Susak, and E. Becker, "Energy expenditure and cardiac response in above-knee amputees while using prostheses with open and locked knee mechanisms.," *Scandinavian journal of rehabilitation medicine. Supplement*, vol. 12, pp. 108–11, 1985.

[16] K. Postema, H. J. Hermens, J. de Vries, H. F. Koopman, and W. H. Eisma, "Energy storage and release of prosthetic feet. Part 1: Biomechanical analysis related to user benefits.," *Prosthetics and orthotics international*, vol. 21, no. 1, pp. 17–27, 1997.

[17] A. Staros, "The SACH (Solid-Ankle Cushion-Heel) Foot," tech. rep., 1957.

[18] P. B. Samuel K. Au and H. Herr, "An EMG-position controlled system for an active ankle-foot prosthesis: An initial experimental study," tech. rep., 2005.

[19] B. J. Hafner, L. L. Willingham, N. C. Buell, K. J. Allyn, and D. G. Smith, "Evaluation of Function, Performance, and Preference as Transfemoral Amputees Transition From Mechanical to Microprocessor Control of the Prosthetic Knee," *Archives of Physical Medicine and Rehabilitation*, vol. 88, no. 2, pp. 207–217, 2007.

[20] F. Sup, A. Bohara, and M. Goldfarb, "Design and Control of a Powered Transfemoral Prosthesis.," *The International journal of robotics research*, vol. 27, no. 2, pp. 263–273, 2008.

[21] H. A. Varol, F. Sup, and M. Goldfarb, "Multiclass real-time intent recognition of a powered lower limb prosthesis.," *IEEE transactions on bio-medical engineering*, vol. 57, no. 3, pp. 542–51, 2010.

[22] M. R. Tucker, J. Olivier, A. Pagel, H. Bleuler, M. Bouri, O. Lambercy, J. D. R. Millán, R. Riener, H. Vallery, and R. Gassert, "Control strategies for active lower extremity prosthetics and orthotics: a review," tech. rep., 2015.

[23] M. R. Pitkin, *Biomechanics of Lower Limb*. Springer-Verlag Berlin, 2010.

[24] P. E. Martin and D. W. Morgan, "Biomechanical considerations for economical walking and running.," *Official Journal of the American College of Sports Medicine*, 1992.

[25] M. A. Holgate, T. G. Sugar, and A. W. BÌĹohler, "A novel control algorithm for wearable robotics using phase plane invariants," *Proceedings - IEEE International Conference on Robotics and Automation*, pp. 3845–3850, 2009.

[26] S. H. Collins, "Dynamic walking principles applied to human gait," *PhD thesis in Mechanical Engineering at University of Michigan*, 2008.

[27] N. L. Dudek, M. B. Marks, S. C. Marshall, and J. P. Chardon, "Dermatologic conditions associated with use of a lower-extremity prosthesis," *Archives of Physical Medicine and Rehabilitation*, vol. 86, no. 4, pp. 659–663, 2005.

[28] H. Meulenbelt, J. Geertzen, P. Dijkstra, and M. Jonkman, "Skin problems in lower limb amputees: an overview by case reports," *Journal of the European Academy of Dermatology and Venereology*, vol. 21, no. 2, pp. 147–55, 2007.

[29] A. G. Hatfield and J. D. Morrison, "Polyurethane gel liner usage in the Oxford Prosthetic Service," *Prosthetics and Orthotics International*, vol. 25, no. 1, pp. 41–46, 2001.

[30] T. Reissman, E. Halsne, R. Lipschutz, L. Miller, and T. Kuiken, "A novel gel liner system with embedded electrodes for use with upper limb myoelectric prostheses," *PLOS ONE*, vol. 13, no. 6, p. e0198934, 2018.

[31] C. L. Vaughan, B. L. Davis, and J. C. O'Connor, "The Three-Dimensional and Cyclic Nature of Gait," *Dynamics of Human Gait*, pp. 16–17, 1999.

[32] J. Perry, "Atlas of limb prosthetics: Surgical, prosthetic, and rehabilitation principles," *American academy of orthopaedic surgeons*, 2002.

[33] K. E. Zelik and P. G. Adamczyk, "A unified perspective on ankle push-off in human walking," *The Journal of Experimental Biology*, vol. 219, no. 23, pp. 3676–3683, 2016.

[34] P. Mahmoodi, R. S. Ransing, and M. I. Friswell, "Modelling the effect of âĂŸ heel to toe ' roll-over contact on the walking dynamics of passive biped robots," *Applied Mathematical Modelling*, vol. 37, no. 12-13, pp. 7352–7373, 2013.

[35] J. Henrickson, J. Valasek, and R. Skelton, "Shape Control of Tensegrity Structures," *AIAA SPACE 2015 Conference and Exposition*, pp. 1–20, 2015.

[36] R. E. Skelton and M. C. de Oliveira, "Optimal complexity of deployable compressive structures," *Journal of the Franklin Institute*, vol. 347, no. 1, pp. 228–256, 2010.

[37] R. Goyal, T. Bryant, M. Majji, R. E. Skelton, and A. Longman, "Design and control of growth adaptable artificial gravity space habitat," in *AIAA SPACE and Astronautics Forum and Exposition*, p. 5141, 2017.

[38] M. Chen, Y. Shen, R. Goyal, M. Majji, and R. E. Skelton, "Energy analysis of growth adaptable artificial gravity space habitat," in *AIAA SPACE and Astronautics Forum and Exposition*, p. 5109, 2018.

[39] R. E. Skelton and M. C. de Oliveira, "Optimal tensegrity structures in bending: the discrete Michell truss," *Journal of the Franklin Institute*, vol. 347, no. 1, pp. 257–283, 2010.

[40] G. Carpentieri, R. E. Skelton, and F. Fraternali, "Minimum mass and optimal complexity of planar tensegrity bridges," *International Journal of Space Structures*, vol. 30, no. 3-4, pp. 221–243, 2015.

[41] R. Goyal, E. A. P. Hernandez, and R. E. Skelton, "Analytical study of tensegrity lattices for mass-efficient mechanical energy absorption," *International Journal of Space Structures*, 2018.

[42] K. Nagase and R. E. Skelton, "Minimal mass tensegrity structures," *Journal of the International Association for Shell and Spatial Structures*, vol. 55, no. 1, pp. 37–48, 2014.

[43] R. Skelton and M. de Oliveira, *Tensegrity Systems*. Springer US, 2009.

[44] H. Karnan, R. Goyal, M. Majji, R. E. Skelton, and P. Singla, "Visual feedback control of tensegrity robotic systems," *2017 IEEE/RSJ International Conference on Intelligent Robots and Systems (IROS)*, pp. 2048–2053, Sept 2017.

[45] J. Cheong and R. E. Skelton, "Nonminimal dynamics of general class k tensegrity systems," *International Journal of Structural Stability and Dynamics*, vol. 15, no. 2, pp. 1–22, 2015.

[46] J. Y. Zhang and M. Ohsaki, "Stability conditions for tensegrity structures," *International Journal of Solids and Structures*, vol. 44, pp. 3875–3886, 2006.

[47] J. L. Crassidis and J. L. Junkins, *Optimal estimation of dynamic systems - Second Edition*. CRC Press US, 2011.

[48] G. Bovi, M. Rabuffetti, P. Mazzoleni, and M. Ferrarin, "A multiple-task gait analysis approach : Kinematic , kinetic and EMG reference data for healthy young and adult subjects," *Gait & Posture*, vol. 33, pp. 6–13, 2011.

[49] R. Goyal and R. E. Skelton, “Dynamics of class 1 tensegrity systems including cable mass,” in *16th Biennial ASCE International Conference on Engineering, Science, Construction and Operations in Challenging Environments.*, 2018.

APPENDIX A

Single Bar Dynamics Consider a vector **r** locating the center of mass of the rod of length $l = |\mathbf{b}|$, where **b** is the vector along the rod.

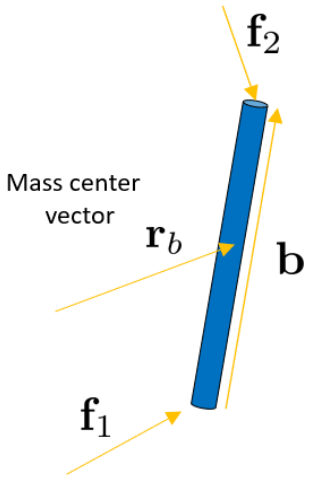

Figure 5.1: Single Bar showing bar vector, external forces (f_1,f_2), center of mass vector(r_b).

Translational Dynamics

$$m\ddot{\mathbf{r}} = \mathbf{f}_1 + \mathbf{f}_2, \tag{5.1}$$

Rotational dynamics Using the Euler equations of motion, we can write the angular momentum expression for the bar about its mass center.

$$\mathbf{h} = I\boldsymbol{\omega} \tag{5.2}$$

$$= \frac{ml^2}{12}\left(\frac{\mathbf{b}\times\dot{\mathbf{b}}}{l^2}\right) \tag{5.3}$$

$$\mathbf{h} = \frac{m}{12}\mathbf{b}\times\dot{\mathbf{b}}, \tag{5.4}$$

Here, we have used the relationship between $\boldsymbol{\omega}$, the angular velocity of rod $\mathbf{b}$, and vectors $\mathbf{b}$ and $\dot{\mathbf{b}}$:

$$\boldsymbol{\omega} = \frac{\mathbf{b}\times\dot{\mathbf{b}}}{\|\mathbf{b}\|^2}. \tag{5.5}$$

The time rate of change of the angular momentum vector $\mathbf{h}$ is equal to the sum of torques τ acting on the rod member about its center of mass. The resulting torques due to the forces illustrated in 5.1, we get:

$$\dot{\mathbf{h}} = \frac{m}{12}\dot{\mathbf{b}}\times\dot{\mathbf{b}} + \frac{m}{12}\mathbf{b}\times\ddot{\mathbf{b}}, \tag{5.6}$$

$$= \frac{m}{12}\mathbf{b}\times\ddot{\mathbf{b}}, \tag{5.7}$$

$$\dot{\mathbf{h}} = \tau, \tag{5.8}$$

$$= \frac{1}{2}\mathbf{b}\times(\mathbf{f}_2 - \mathbf{f}_1). \tag{5.9}$$

$$\frac{m}{12}\tilde{\mathbf{b}}\ddot{\mathbf{b}} = \frac{1}{2}\tilde{\mathbf{b}}(\mathbf{f}_2 - \mathbf{f}_1). \tag{5.10}$$

where $\tilde{\mathbf{a}}$ expresses a skew symmetric matrix formed by the components of vector $\mathbf{a}$.

Since, the bars are considered rigid in this formulation, the length (l) of the bars do not get

altered.

$$\mathbf{b}^T\mathbf{b} = l^2 \tag{5.11}$$

On differentiating the constant length constraint of Equation 5.11 twice and appending it with the derived rotational dynamics in equation 5.10, we get:

$$\dot{\mathbf{b}}^T\mathbf{b} + \mathbf{b}^T\dot{\mathbf{b}} = 0 = 2\mathbf{b}^T\dot{\mathbf{b}} \tag{5.12}$$

$$\mathbf{b}^T\ddot{\mathbf{b}} = -\dot{\mathbf{b}}^T\dot{\mathbf{b}}. \tag{5.13}$$

The length constraint (Equation 5.13) and rotational dynamics (Equation 5.10), both in terms of $\ddot{\mathbf{b}}$ can be re-expressed in matrix form as:

$$\begin{bmatrix} \tilde{\mathbf{b}} \\ \mathbf{b}^T \end{bmatrix} \ddot{\mathbf{b}} = \begin{bmatrix} \frac{6}{m}\tilde{\mathbf{b}}(\mathbf{f}_2 - \mathbf{f}_1) \\ -\dot{\mathbf{b}}^T\dot{\mathbf{b}} \end{bmatrix}. \tag{5.14}$$

The above equation can be expressed as a linear algebra problem, AX=Y. The solution to which exists if Y lies in the range space of A. Once we know the solution to this equation exists at any time 't' for any given external forces f_1 and f_2 which it does as proved in [45], we can say that the solution is unique owing to the full column rank attribute of A at every time instant. Therefore, denoting a matrix pseudo inverse by the superscript "+", the unique solution for $\ddot{\mathbf{b}}$ is:

$$\ddot{\mathbf{b}} = \begin{bmatrix} \tilde{\mathbf{b}} \\ \mathbf{b}^T \end{bmatrix}^+ \begin{bmatrix} \frac{6}{m}\tilde{\mathbf{b}}(\mathbf{f}_2 - \mathbf{f}_1) \\ -\dot{\mathbf{b}}^T\dot{\mathbf{b}} \end{bmatrix} \tag{5.15}$$

$$= \frac{1}{l^2}[-\frac{6}{m}\tilde{\mathbf{b}}\tilde{\mathbf{b}}(\mathbf{f}_2 - \mathbf{f}_1) - \mathbf{b}\dot{\mathbf{b}}^T\dot{\mathbf{b}}] \tag{5.16}$$

Since, $\tilde{\mathbf{b}}\tilde{\mathbf{b}} = -l^2 I + \mathbf{b}\mathbf{b}^T$. Rearranging Equation 5.16 gives the final form of the vector equations

for rotational dynamics:

$$\frac{m}{12}\ddot{\mathbf{b}} = -\frac{1}{2l^2}\mathbf{b}\mathbf{b}^T(\mathbf{f}_2 - \mathbf{f}_1) + \frac{1}{2}(\mathbf{f}_2 - \mathbf{f}_1) - \frac{m}{12l^2}\mathbf{b}\dot{\mathbf{b}}^T\dot{\mathbf{b}}. \tag{5.17}$$

Matrix Formulation for the Structure Dynamics We have defined the dynamics for a single bar in the previous section. Now, we can make use of certain connectivity matrices to describe the full network of a tensegrity structure with β rod members and σ strings and write the dynamics for the entire structure in a matrix form.

On defining the string connectivity matrix by C_S^T, and the rod connectivity matrix by C_B^T, we can aggregate all individual bars and strings into a bar matrix ($B = NC_B^T$) and a string matrix ($S = NC_S^T$) . Additionally, we define a matrix to express all the inertial position vectors of the center of mass of β bars as $R = NC_R^T$.

For any n-dimensional column vector, the“hat" operator over a vector is defined to provide a diagonal matrix from the elements of the vector and the $\lfloor\circ\rfloor$ operator, which sets every off-diagonal element of the square matrix operand to zero [49].

$$\frac{1}{2}(\mathbf{f}_{2_i} - \mathbf{f}_{1_i}) = \frac{1}{2}[FC_B^T]_i, \tag{5.18}$$

On implementing the above equation in 5.10 where F contains the the net force vectors $[f_1, f_2.....f_{2\beta}]$ acting on every node, we get:

$$\ddot{B}\frac{\hat{m}}{12} = \frac{1}{2}FC_B^T - \frac{1}{2}B\hat{l}^{-2}\lfloor B^T FC_B^T\rfloor - B\frac{\hat{m}}{12}\hat{l}^{-2}\lfloor\dot{B}^T\dot{B}\rfloor \tag{5.19}$$

On the introduction of a new variable $\hat{\lambda}$, the above expression is further simplified into:

$$\hat{\lambda} = -\frac{\hat{m}}{12}\hat{l}^{-2}\lfloor\dot{B}^T\dot{B}\rfloor - \frac{1}{2}\hat{l}^{-2}\lfloor B^T FC_B^T\rfloor \tag{5.20}$$

$$\ddot{B}\frac{\hat{m}}{12} = \frac{1}{2}FC_B^T + B\hat{\lambda}, \tag{5.21}$$

The matrix expressions for the rotational and translational dynamics of the full tensegrity system can be represented as:

$$\begin{bmatrix} \ddot{B} & \ddot{R} \end{bmatrix} \begin{bmatrix} \frac{\hat{m}}{12} & 0 \\ 0 & \hat{m} \end{bmatrix} + \begin{bmatrix} B & R \end{bmatrix} \begin{bmatrix} -\hat{\lambda} & 0 \\ 0 & 0 \end{bmatrix} = F \begin{bmatrix} \frac{1}{2}C_B^T & 2C_R^T \end{bmatrix}. \tag{5.22}$$

Using $\begin{bmatrix} \frac{1}{2}C_B^T & 2C_R^T \end{bmatrix}^{-1} = \begin{bmatrix} C_B^T & C_R^T \end{bmatrix}^T$, we get:

$$\begin{bmatrix} \ddot{B} & \ddot{R} \end{bmatrix} \begin{bmatrix} \frac{\hat{m}}{12}C_B \\ \hat{m}C_R \end{bmatrix} + \begin{bmatrix} B & R \end{bmatrix} \begin{bmatrix} -\hat{\lambda}C_B \\ 0 \end{bmatrix} = F. \tag{5.23}$$

On expanding the above equations by including the node matrices and connectivity matrices leads:

$$\ddot{N}(C_B^T \frac{\hat{m}}{12} C_B + C_R^T \hat{m} C_R) - N(C_B^T \hat{\lambda} C_B) = F. \tag{5.24}$$

The tension vector in a string can be found as $\mathbf{t}_i = \mathbf{s}_i \gamma_i$ where $\mathbf{s}_i$ is associated with the i^{th} column of matrix S and γ can be read as normalized tension. Therefore, the internal forces acting on nodes caused by string tensions are $NC_S^T \hat{\gamma} C_S$ which can be used to form a force matrix expression which on substitution into Equation 5.24 leads:

$$F = W - NC_S^T \hat{\gamma} C_S \tag{5.25}$$

$$\ddot{N}(C_B^T \frac{\hat{m}}{12} C_B + C_R^T \hat{m} C_R) + N(C_S^T \hat{\gamma} C_S - C_B^T \hat{\lambda} C_B) = W \tag{5.26}$$

Finally, a simplified expression for dynamics of Tensegrity structures can be formulated as:

$$\ddot{N}M + NK = W \tag{5.27}$$

$$K = C_S^T \hat{\gamma} C_S - C_B^T \hat{\lambda} C_B \tag{5.28}$$

$$M = C_B^T \frac{\hat{m}}{12} C_B + C_R^T \hat{m} C_R \tag{5.29}$$

Class K dynamics All Class k ($k > 1$) joints are converted into k Class 1 nodes which are constrained to coincide at all times with the help of Lagrange multipliers using the constraint equation as:

$$NP = D, \tag{5.30}$$

where P is a $n \times c$ and D is a $3 \times c$ matrix with c denoting the number of constraints. On incorporating the resulting constraint forces denoted by Ω into the dynamics, we get

$$\ddot{N}M + NK = W + \Omega P^T \tag{5.31}$$

where

$$K = \left[C_S^T \hat{\gamma} C_s - C_B^T \hat{\lambda} C_B \right], \tag{5.32}$$

$$\hat{\lambda} = -\frac{\hat{m}}{12}\hat{l}^{-2}\lfloor \dot{B}^T \dot{B} \rfloor - \frac{1}{2}\hat{l}^{-2}\lfloor B^T (W + \Omega P^T - S\hat{\gamma} C_S) C_B^T \rfloor, \tag{5.33}$$

and Ω is the $3 \times c$ matrix of Lagrange multipliers.

The dynamics Equation 5.31 can be reduced into a smaller dimensional equation by augmenting it with the constraint Equation 5.30. Singular value decomposition (SVD) of matrix P can be done as:

$$P = U\Sigma V^T = \begin{bmatrix} U_1 & U_2 \end{bmatrix} \begin{bmatrix} \Sigma_1 \\ 0 \end{bmatrix} \begin{bmatrix} V^T \end{bmatrix} \tag{5.34}$$

where $U \in \mathbf{R}^{n \times n}$ and $V \in \mathbf{R}^{c \times c}$ are both unitary matrices, and $\Sigma_1 \in \mathbf{R}^{c \times c}$ is a diagonal matrix of positive singular values. By defining

$$[\eta_1 \;\; \eta_2] = [NU_1 \;\; NU_2], \tag{5.35}$$

the constraint Equation 5.30 can be modified as:

$$NU\Sigma V^T = [\eta_1 \;\; \eta_2] \begin{bmatrix} \Sigma_1 \\ 0 \end{bmatrix} \begin{bmatrix} V^T \end{bmatrix} = D, \tag{5.36}$$

Recognizing,

$$\eta_1 = DV\Sigma_1^{-1}, \;\; \dot{\eta}_1 = 0, \;\; \ddot{\eta}_1 = 0. \tag{5.37}$$

we can say, η_1 represents the space with zero motion in transformed coordinates and η_2 can be used to write the dynamical equations in the reduced subspace. Using Equations 5.34-5.37, the dynamics equation 5.31 can be rewritten as:

$$\ddot{N}UU^TM + NUU^TK = W + \Omega V\Sigma^TU^T \tag{5.38}$$

$$\ddot{\eta}_2U_2^TM + \eta_1U_1^TK + \eta_2U_2^TK = W + \Omega V\Sigma_1^TU_1^T. \tag{5.39}$$

Post-multiplying the above equation by $[U_2 \;\; M^{-1}U_1]$ yields

$$\ddot{\eta}_2U_2^TMU_2 + \eta_2U_2^TKU_2 = WU_2 - \eta_1U_1^TKU_2 \tag{5.40}$$

$$NKM^{-1}U_1 - \Omega P^TM^{-1}U_1 = WM^{-1}U_1. \tag{5.41}$$

First equation in 5.41 is used as the dynamics equation for tensegrity structures in the reduced space while the second equation is linear in the Lagrange multiplier (Ω) and is used for its evaluation. One can see K is also a function of Ω, making it a linear algebra problem.